이학박사 학위논문

NaCl Effect and Its Molecular Mechanism on the Dielectric Constant of Nanoconfined Water Studied by Dielectric Relaxation Spectroscopy

유전체 이완 분광법을 이용한 나노 공간에 갇힌 물의 유전 상수에 대한 NaCl 효과와 그 메커니즘 연구

2021년 8월

서울대학교 대학원

물리천문학부 물리학 전공

장정민

NaCl Effect and Its Molecular Mechanism on the Dielectric Constant of Nanoconfined Water Studied by Dielectric Relaxation Spectroscopy

지도 교수 박 혜 윤

이 논문을 이학박사 학위논문으로 제출함

2021년 8월

서울대학교 대학원

물리천문학부 물리학 전공

장정민

장정민의 이학박사 학위논문을 인준함

2021년 8월

위 원 장 최 현 용

부위원장 박 혜 윤

위 원 백 용 주

위 원 박 건 식

위 원 박 재 헌

Abstract

NaCl Effect and Its Molecular Mechanism on the Dielectric Constant of Nanoconfined Water Studied by Dielectric Relaxation Spectroscopy

Jeongmin Jang
Department of Physics and Astronomy
The Graduate School of Seoul National University

In this study, we suggest the first experimental evidence that NaCl enhances the dielectric constant of nanoconfined water in phospholipid multilamellar vesicles (MLVs) using GHz dielectric relaxation spectroscopy (DRS). Such phenomenon was not observed in the bulk environments (Bulk NaCl solution or phospholipid micelle/NaCl solution), in which monotonic reduction of the dielectric constant with increasing salt concentration was revealed. NaCl induces non-linear change of the static permittivity of water confined in MLVs, namely an anomalous increase near the physiological salt concentration ($0 < c < 0.3$ M) and a decrease at high concentration ($0.3 < c < 1$ M). Comparing with previous simulations' results, this non-linear behavior is interpreted as a result of competition between the increase of the perpendicular dielectric component ($\varepsilon_{\perp}$) and the decrease of the parallel dielectric component ($\varepsilon_{\parallel}$) on the membrane surface induced by NaCl.

In addition, the molecular mechanism of the abnormal NaCl effect is also investigated. NaCl enhances the dielectric constant of two water regions in MLVs, i.e., membrane-surface bound water and water beyond it, in a different way. Accelerated collective reorientation motion of surface-bound water was observed, which implies an increase of rotational freedom. For water beyond the hydration layer, however, slower collective motion and an increase in dielectric constant were simultaneously observed, suggesting a novel mechanism by which NaCl enhances

the intermolecular orientation correlation (or Kirkwood correlation factor, g_K) rather than rotational freedom of individual water molecules.

Keywords: Nanoconfined water, NaCl, dielectric constant, phospholipid, Kirkwood correlation factor, intermolecular orientation correlation, dielectric relaxation spectroscopy

Student Number: 2016-30098

DEDICATION

To my parents, the source of endless love and support.

장양관, 모혜순님의 헌신과 사랑에 깊은 감사를 드립니다.

Contents

Abstract ..... **i**

Chapter 1. Introduction **1**

1.1 Research Background 1

1.2 Questions that are covered in This Thesis 3

Bibliography 4

Chapter 2. Theoretical Background **5**

2.1 Fundamental Equations 5

2.1.1 Maxwell Equations 5

2.1.2 Dielectric Constant with Free Charge 6

2.2 Dielectric Relaxation Model 8

2.2.1 Dielectric Response 8

2.2.2 Debye Relaxation Model 9

2.3 Dipole-Dipole Oreintational Correlation 13

2.3.1 Kirkwood-Frohlich Model 13

2.3.2 Kivelson-Madden Model 15

2.4 Effective Medium Theory 17

2.4.1 Overview 17

2.4.2 Bruggeman Mxture Model 17

Bibliography 19

Chapter 3. Methods and Materials **20**

3.1 Dielectric Relaxation Spectroscopy (DRS) 20

3.1.1 Overview 20

3.1.2 Open-Ended Coaxial Probe Method 22

3.1.3 Bilinear Model 24

3.1.4 Experimental Setup 27

3.2 Small Angle X-ray Scattering 29

3.2.1 Principle 29

3.2.2 Experimental Setup 31

3.3 Conductivity of NaCl/lipid Aqueous Solution 33
3.4.1 Principle 33
3.4.2 Experimental Setup 34
3.4 Sample 35
3.5.1 Lipids 35
3.5.2 Self-Assembly Structures 37
3.5.3 Sample Preperation 39
Bibliography 40

Chapter 4. Observation of Nano Space insde Lipid Multilmaellar Vesicle (MLV) 41
4.1 MLV Repeat Distance of DMPC/NaCl Solution 41
Bibliography 44

Chapter 5. Observation of Anomalous NaCl Effect on the Dielectric Constant of Nanoconfined Water in MLVs 45
5.1 Obtaing Process of Dielectric Constant of All Samples 45
5.2 Anomalous Increase of Dielectric Constant in DMPC/NaCl Solution (Raw Data) 51
5.3 Effective Medium Approximation 57
5.4 Anomalrous Increase of Dielectric Constant of Nanoconfined NaCl Solution (in DMPC MLV) 61
5.5 Interpretation 64
Bibliography 66

Chapter 6. Molecular Mehcanism of NaCl Effect on Dielectric Constant of Confined Water in MLVs 67
6.1 For Membrane-Surface Bound Water 67
6.2 For Water Beyond Membrane Hydation Layer 71
Bibliography 75

Chapter 7. Conclusion 76

국문초록 77

List of Figures

Figure 2.1. Schematics of rotational diffusion of permanent dipole moment under the applied electric field 9
Figure 2.2. Concept of Kirkwood-Frohlich model... 13
Figure 2.3. Concept of effective medium theory.. 17
Figure 2.4. Electric flux inside the material which composed by two different components 18
Figure 3.1. Frequency response of dielectric polarization of typical polar liquids. 20
Figure 3.2. Various methods for measuring the dielectric constant of different kinds of samples over a wide frequency range. 22
Figure 3.3. Schematics of reflection coefficient measurement using open-ended coaxial probe 23
Figure 3.4. Schematics of two port network system. 23
Figure 3.5. Schematics of equivalent circuit of probe-sample interface. .. 24
Figure 3.6. Equivalent circuit with scattering matrix 26
Figure 3.7. Open-ended coaxial probe connected to vector network analyzer for 0.1-70 GHz dielectric measurement. 28
Figure 3.8. Bragg's law. 29
Figure 3.9. Schematics of SAXS measurement on lamellar repeat distance in lipid vesicle. 30
Figure 3.10. Two types of X-ray beam for SAXS measurement 30
Figure 3.11. Experimental setup for SAXS (Wonkwang University) 31
Figure 3.12. Scattered line-collimated beam from lipid MLVs is detected in 2D CCD camera 32
Figure 3.13. Schematics of measurement of DC conductivity of electrolyte solution 33
Figure 3.14. Experimental setup for ion conductivity measurement of liquid samples 34

Figure 3.15. Amphiphilic property of a lipid molecule 35
Figure 3.16. Lipid self-assembly process 36
Figure 3.17. Lipid self-assembly structures depending on packing parameter 38
Figure 3.18. Sample preparation of lipid/NaCl solution 39
Figure 4.1. Scattering vector vs. scattering intensity for DMPC/NaCl solutions 41
Figure 4.2. Lamellar repeat distance (d) of DMPC MLV for different NaCl concentrations 42
Figure 5.1. (a) Measured total dielectric loss, (b) After subtraction of ionic conductivity term from (a) 45
Figure 5.2. Scheme of conductivity measurement on DMPC/NaCl solution by conductivity meter 46
Figure 5..3. Increment of dielectric loss ($\boldsymbol{\varepsilon''}$) at 3 GHz for all samples as a function of NaCl concentration 47
Figure 5.4. NaCl conductivity of all samples 48
Figure 5.5. Dielectric loss of DMPC/NaCl sample after subtracting ion conductivity from measured total dielectric loss 48
Figure 5.6. Dielectric loss ($\boldsymbol{\varepsilon''}$) of all samples. Dielectric loss of (a) water, LMPC/water, DMPC/water, (b) NaCl, (c) LMPC/NaCl and (d) DMPC/ NaCl 49
Figure 5.7. Permittivity ($\boldsymbol{\varepsilon'}$) of all samples. Permittivity of (a) NaCl, (b) LMPC/NaCl and (c) DMPC/ NaCl 50
Figure 5.8. Dielectric loss spectrum, four Debye relaxation mode fit (black solid line), and their mode decomposition for (a) LMPC/water and (b) DMPC/water. 52
Figure 5.9. (a) Dielectric strengths and (b) relaxation times of bulk mode for all samples 54
Figure 5.10. (a) Change of permittivity of all samples at 10 GHz with NaCl concentration, (b) Focus on NaCl low concentration. 55

Figure 5.11. Structure inside MLV: MLV is composed by periodic unit cells 57
Figure 5.12. After centrifugation of DMPC/NaCl solution: (a) In 0.3 M NaCl solution, (b) In 0.6 M NaCl solution 58
Figure 5.13. $\boldsymbol{f_{MLV}}$ obtained by two different method 59
Figure 5.14. $\boldsymbol{\varepsilon^*_{MLV}}$ obtained from Bruggeman mixture model with three difference conditions. (a) Permittivity, (b) Dielectric loss. Solid line: Fitting by four Debye relaxation model. 60
Figure 5.15. (a) Permittivity and (b) Dielectric loss spectrum of DMPC MLV for different NaCl concentrations obtained by Bruggeman mixture model (Solid line: Four Debye fitting result). 62
Figure 5.16. Static permittivity for NaCl solution confined in DMPC MLV (Black open diamond) and volume corrected value (red filled diamond). The dark red dashed line denotes a value of nanoconfined water (~ 45.5). Values for water and bulk NaCl solution were also represented (Black solid line and black open circle, respectively). 63
Figure 5.17. Open-ended coaxial probe method measures "average" of all dielectric components in DMPC MLVs. 64
Figure 5.18. Static permittivity of our data (NaCl in MLVs, red diamond) is compared to $((\boldsymbol{\varepsilon_\perp + \varepsilon_\parallel})/\mathbf{2})$ of nanoconfined NaCl solution btw two graphene layers 65
Figure 6.1. (a) Dielectric strengths and (b) relaxation times of both tightly and weakly bound water for NaCl solution inside DMPC MLV, respectively. 68
Figure 6.2. (a) Dielectric strengths and (b) relaxation times of both tightly and weakly bound water for LMPC/NaCl solution, respectively. 69
Figure 6.3. Schematics of NaCl effect on tightly bound water of DMPC membrane. 70
Figure 6.4. (a) Dielectric strengths, relaxation times, and (b) Kirkwood factor of water beyond the membrane-surface bound water for NaCl solution confined in DMPC MLV. Data for NaCl in the bulk system is also represented.

.....72
Figure 6.5. Schematics of NaCl effect on intermolecular orientation correlation beyond membrane hydration layer. 74

Chapter 1.
Introduction

1.1 Research Background

Aqueous electrolyte solutions confined to nanoscale spaces are ubiquitous in biological systems and nano devices, such as the crowding interior of living cells, ion channels in cell membranes, multilayered lipid bilayers (e.g., human stratum corneum, mitochondria, myelin sheath and chloroplast), human joints, desalination membranes and super capacitors. Therefore, the physical and chemical properties of aqueous nanoconfined electrolyte solutions have been intensively investigated to understand their biological functions or to design nano devices. In particular, the dielectric constant is one of the important properties in various biochemical and electrochemical processes such as ion hydration, ion transport, chemical reaction, protein folding, macromolecular aggregation, desalination, and capacitance, as it directly determines the strength of the water-mediated intermolecular force in an aqueous environment.

Recent molecular dynamics simulation studies have shown that nanoconfined aqueous NaCl solutions have anomalous dielectric behaviors compared to bulk solutions. For example, anisotropic dielectric constant and an increase in the dielectric component perpendicular to the platform surface with increasing ion concentration have been proposed [1-3]. The latter was considered particularly abnormal, and the molecular origin has been intensively investigated because it has been very well known for 100 years that ions monotonically reduce the dielectric constant of bulk water [4-8] due to the “dielectric saturation effect” where ion weaken intermolecular orientation correlation in the surrounding water dipoles [9] by inducing orientational alignment [10-11]. However, experimental evidence for such abnormal dielectric behavior is still lacking.

The molecular mechanism by which ions enhances the dielectric constant of confined water is still not fully understood. The strength of the dielectric constant of polar liquids is dominantly determined by the reorientation response of permanent dipole moments to the applied electric field [12]. Therefore, to reveal the molecular

mechanism, how ion affects the rotational degree of freedom of confined water has been mainly investigated. In the previous simulation studies, it has been commonly suggested that the ionic perturbation effect enhances the rotational degree of freedom of water molecules pre-oriented in a direction perpendicular to the platform surface, which is the main origin for the enhancement of the dielectric constant of the confined aqueous solution. Such a scenario has been supported by the fact that NaCl randomizes the orientation of water dipoles [2-3], reduces hydrogen bond (H-bond) lifetime, and accelerates dielectric relaxation time [1]. However, since water molecules are strongly linked with each other by H-bonds, water dipoles have correlated reorientation motion and which effectively enhances the dielectric constant of liquid water [13-14]. The degree of dipole-dipole orientation correlation is generally quantified as a Kirkwood correlation factor (also called as a dielectric enhancement factor, g_K), where liquid water has a higher intermolecular correlation (g_K=2.7 [9, 15]) than random orientated structure (g_K=1). Despite such a significance, to the authors' knowledge, no studies have yet investigated the molecular mechanism of enhanced dielectric constant in terms of modification of intermolecular correlation. Moreover, it is still not clear whether the molecular origin is consistent in all water molecular regions of the confined environment or differs in interfacial water and beyond it.

Dielectric relaxation spectroscopy (DRS) is a suitable experimental method for investigating the anomalous dielectric behavior of nanoconfined ionic solutions and revealing its further molecular origin because it can simultaneously probe the dielectric constant and intermolecular orientation correlation of confined water. DRS has an inherent ability to probe the collective reorientation motion of dipole moments, providing information on the orientation correlation (g_K) [14-15]. For example, a recent DRS methodologies have shown that the perturbation such as ions or nanoconfinement can significantly reduce g_K of liquid water [9, 16-17]. In addition, DRS has successfully decomposed the different reorientation time of surface-bound water and bulk water [18-19]. Therefore, using this method, it is expected that the molecular mechanisms for the interfacial water and the water beyond it will be separately investigated.

In this thesis, we investigate how the NaCl affects the dielectric constant of nanoconfined water inside phospholipid multilamellar vesicle (DMPC MLV).

Phospholipids is well known as important components of cell membranes (> 75% of total lipids [20]), so it is considered as an useful platform for mimicking bio systems. To understand the molecular mechanisms, change in collective reorientation dynamics is studied for both the membrane surface-bound water and water beyond it. Finally, the Kirkwood correlation factor (g_K) is analyzed from the dielectric strength and the collective relaxation time. The result is compared with those in the phospholipid micelle (LMPC)/NaCl solution, which has the same surface as the MLV but no nano space.

1.2 Questions that are covered in This Thesis

- How NaCl affects the dielectric constant of nanoconfined water in phospholipid MLVs? (Chapter 5)
- Is the Molecular mechanism of NaCl effect consistent in all water regions in MLVs or not? (Chapter 6)
- What is the mechanism in membrane-surface bound water? (Chapter 6)
- What is the mechanism in water beyond hydration layer? (Chapter 6)

Bibliography

1. Zhu, H.; Ghoufi, A.; Szymczyk, A.; Balannec, B.; Morineau, D., *Phys. Rev. Lett.* **2012,** *109* (10).
2. Renou, R.; Szymczyk, A.; Ghoufi, A., *Nanoscale* **2015,** *7* (15), 6661-6666.
3. Jalali, H.; Lotfi, E.; Boya, R.; Neek-Amal, M., *J. Phys. Chem. B* **2021,** *125* (6), 1604-1610.
4. Lattey, R. T., *The London, Edinburgh, and Dublin Philosophical Magazine and Journal of Science* **1921,** *41* (246), 829-848.
5. Schmidt, C. C., *Phys. Rev.* **1927,** *30* (6), 925-930.
6. Kaatze, U., *J. Solution Chem.* **1997,** *26* (11), 1049-1112.
7. Buchner, R.; Hefter, G. T.; May, P. M., *J. Phys. Chem. A* **1999,** *103* (1), 1-9.
8. Eiberweiser, A.; Buchner, R., *J. Mol. Liq.* **2012,** *176*, 52-59.
9. Rinne, K. F.; Gekle, S.; Netz, R. R., *J. Phys. Chem. A* **2014,** *118* (50), 11667-77.
10. Mancinelli, R.; Botti, A.; Bruni, F.; Ricci, M. A.; Soper, A. K., *J. Phys. Chem. B* **2007,** *111* (48), 13570-13577.
11. Stirnemann, G.; Wernersson, E.; Jungwirth, P.; Laage, D., *J. Am. Chem. Soc.* **2013,** *135* (32), 11824-31.
12. Debye, P. J. W., *Polar Molecules*. The Chemical Catalog Company: **1929**.
13. Bottcher, C. J., *Theory of Electric Polarization, Vol.1 Dielectrics in Static Fields*. 2nd ed.; Ch. 6 Elsevier, Amsterdam: **1973**.
14. Kaatze, U., *J. Chem. Phys.* **2017,** *147* (2), 024502.
15. Buchner, R.; Barthel, J.; Stauber, J., *Chem. Phys. Lett.* **1999,** *306*, 57-63.
16. Eom, K. Collective dynamics of nanoconfined water studied by broadband dielectric relaxation spectroscopy. Chapter 4 Ph.D. thesis, Seoul National University, **2019**.
17. Honegger, P.; Schmollngruber, M.; Steinhauser, O., *Phys. Chem. Chem. Phys.* **2018,** *20* (16), 11454-11469.
18. Cametti, C.; Marchetti, S.; Gambi, C. M. C.; Onori, G., *J. Phys. Chem. B* **2011,** *115* (21), 7144-7153.
19. George, D. K.; Charkhesht, A.; Hull, O. A.; Mishra, A.; Capelluto, D. G. S.; Mitchell-Koch, K. R.; Vinh, N. Q., *J. Phys. Chem. B* **2016,** *120* (41), 10757-10767.
20. Vance, J. E., *Traffic* **2015,** *16* (1), 1-18.

Chapter 2.
Theoretical Background

2.1 Fundamental Equations

2.1.1 Maxwell Equations

Electromagnetic phenomena are governed by Maxwell's equations

$$\vec{\nabla} \cdot \vec{D} = \rho \tag{2.1}$$

$$\vec{\nabla} \cdot \vec{B} = 0 \tag{2.2}$$

$$\vec{\nabla} \times \vec{E} = -\frac{\partial \vec{B}}{\partial t} \tag{2.3}$$

$$\vec{\nabla} \times \vec{H} = \vec{j} + \frac{\partial \vec{D}}{\partial t} \tag{2.4}$$

where $\vec{E}$ and $\vec{H}$ are electric and magnetic field strength, respectively, $\vec{D}$ and $\vec{B}$ are electric displacement field and magnetic flex density, respectively, and $\vec{j}$ is the current density. Gauss's law of electric field (Equation 2.1) states that in a closed surface, the total electric flux through that surface is proportional to the total charge contained within it. Equation 2.1 (Gauss's law of magnetic field) is an expression for the fact that the magnetic flux has no monopole. Faraday's law of electro-magnetic induction (Eq. 2.3) describes the generation of electric field when the magnetic flux passing through a closed circuit changes. Eq. 2.4 (Ampere-Maxwell's law) states that magnetic fields can be generated in two ways: by electric current and by changing electric fields. When we combines equation 2.3 and 2.4, electromagnetic wave equation is driven,

$$\vec{\nabla}^2\vec{E} = \mu\varepsilon\frac{\partial^2\vec{E}}{\partial t^2} = \frac{1}{v^2}\frac{\partial^2\vec{E}}{\partial t^2} \quad (2.5)$$

where μ and ε are permeability and dielectric constant, respectively, and v is speed of light in the matter. In the dielectrics, where negligible permeability, equation 2.5 can be simply written as,

$$\vec{\nabla}^2\vec{E} = \frac{\varepsilon_r}{c^2}\frac{\partial^2\vec{E}}{\partial t^2} \quad (2.6)$$

where c is speed of light in the vacuum.

2.1.2 Dielectric Constant with Free Charge (or ions)

When ions are dissolved in solution, applied electric field will induce ionic movement, which causes energy loss in the dielectric. Combining equation 2.3 and 2.4, we obtain,

$$\nabla^2\vec{E} = \mu\frac{\partial}{\partial t}(\vec{J_f} + \frac{\partial\vec{D}}{\partial t}) \quad (2.7)$$

where $\vec{J_f}$ is the current density by free charge (or ions). When using the well-known Ohm's law ($\vec{J_f} = \kappa\vec{E}$, where κ is electric conductivity), equation 2.7 can be written as,

$$\nabla^2\vec{E} = \mu\frac{\partial}{\partial t}(\kappa\vec{E} + \frac{\partial\vec{D}}{\partial t}) \quad (2.8)$$

$$\nabla^2\vec{E} = \frac{\varepsilon_r}{c^2}\frac{\partial^2\vec{E}}{\partial t^2} + \mu_0\kappa\frac{\partial\vec{E}}{\partial t} \quad (2.9)$$

When inserting the solution of wave equation, $\vec{E} \propto e^{i(\vec{k}\cdot\vec{r}-\omega t)}$, into equation 2.9, we get the below relation,

$$k^2 = \frac{\omega^2}{c^2}(\varepsilon + \frac{i\kappa}{\varepsilon_0 \omega}) \quad (2.10)$$

where k and ε_0 are wave vector and permittivity in the vacuum, respectively. When inserting the solution of wave equation, $\vec{E} \propto e^{i(\vec{k}\cdot\vec{r}-\omega t)}$), into equation 2.6, we get an another relation,

$$k^2 = \frac{\omega^2}{c^2}\varepsilon^{tot} \quad (2.11)$$

By combining equation 2.10 and 2.11, we get the relation between the dielectric constant and ionic conductivity in the system,

$$\varepsilon^{tot} = \varepsilon + \frac{i\kappa}{\varepsilon_0 \omega} \quad (2.12)$$

Equation 2.12 suggests that ion movement by applied electric field contributes the experimentally measured dielectric constant (ε^{tot}). Therefore, to study the dielectric constant of the matter only, ionic conductivity term (κ) should be excluded from total dielectric constant.

2.2 Dielectric Relaxation Model

2.2.1 Dielectric Response

When electric field is applied to the polar material, permanent dipole moments reorient and align to applied field (=orientation polarization, $\vec{\mu}$) and electron shell of atom is shifted relative to the nucleus (=distortion polarization, $\alpha\vec{E}$), which phenomena is called "polarization ($\vec{P} = \sum(\vec{\mu} + \alpha\vec{E})$)". The strength of dielectric response is represented as electric susceptibility (χ_e) or dielectric constant (ε),

$$\vec{P} = \varepsilon_0 \chi_e \vec{E} = \varepsilon_0(\varepsilon - 1)\vec{E} \tag{2.13}$$

Since polarization does not respond instantaneously to an external electric field, the general definition can be written as follows,

$$\vec{P}(\mathrm{t}) = \varepsilon_0 \int_{-\infty}^{t} \chi_e(t - t')\, \vec{E}(t')dt' \tag{2.14}$$

where $\chi_e(t - t')$ is time dependent susceptibility. After Fourier transform, polarization in the frequency domain is defined,

$$\vec{P}(\omega) = \varepsilon_0 \chi_e(\omega)\vec{E}(\omega) = \varepsilon_0(\varepsilon(\omega) - 1)\vec{E}(\omega) \tag{2.15}$$

Equation 2.15 implies that information about molecular behaviors (permanent dipole and induced dipole) can be obtained from the macroscopic quantity (ε) and which is essence of dielectric relaxation spectroscopy. In the next section, the theory (Debye equation) will be driven which gives the relation between rotational diffusion dynamics of dipole moments and the dielectric constant.

2.2.2 Debye Relaxation Model

In this section, we will discuss in detail how quantitatively describes the rotational motion of polar molecules from the dielectric constant. In 1929, P. Debye driven the relation between the dielectric constant of the polar matter and rotational diffusion time of permanent dipoles [1]. Polar molecules have a permanent dipole moment and it tends to align with respect to an external electric field. When the external electric field is suddenly turned off, the polar molecules reorient again in a random direction. Therefore, information about the rotational motion of polar molecules can be obtained through rotational response of dipole to applied field, i.e., orientational polarization.

Let's consider a situation in which polar molecules are constantly rotating due to thermal collision under a local electric field $\vec{F}$. In this case, let θ be the angle between the direction of the dipole moment of the polar molecule and the applied electric field (Figure 2.1).

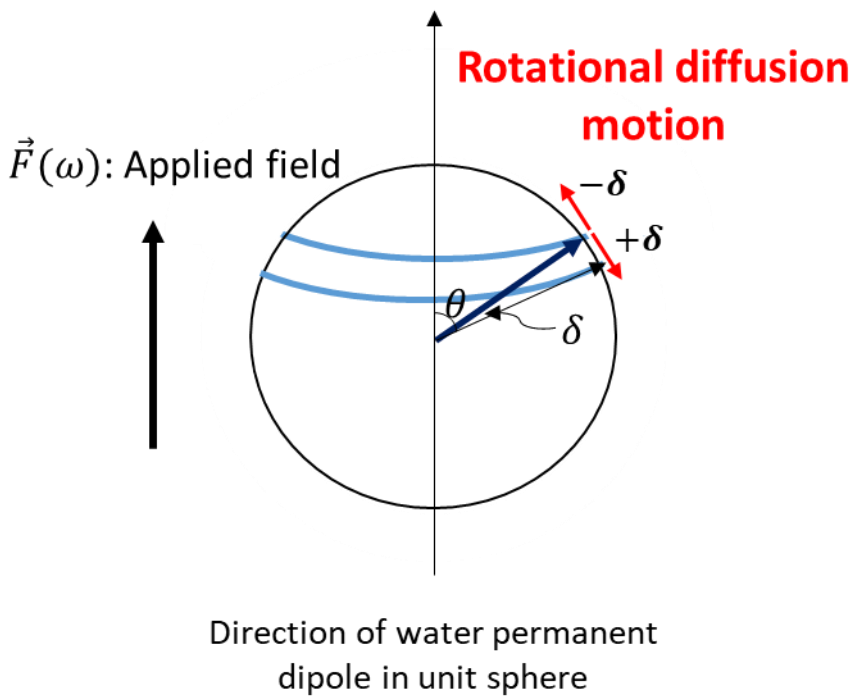

Figure 2.1. Schematics of rotational diffusion of permanent dipole moment under the applied electric field, $\vec{F}$.

The net number of dipole moments entering the solid angle $d\Omega$ during time δt is as below,

$$\delta t \frac{\delta f(\theta,\phi)}{\partial t} d\Omega = \Delta_1 + \Delta_2 \tag{2.16}$$

where $f(\theta,\phi)$ is the distribution function in the direction of the dipole moment, Δ_1 is the contribution of the electric field F and Δ_2 is the contribution of the thermal collision to the rotational motion. Through mathematical calculations of the two contributions, a differential equation for the distribution function $f(\theta,\phi)$ is obtained [1],

$$\zeta \frac{\partial f}{\partial t} = \frac{1}{sin\theta} \frac{\partial}{\partial \theta} \left[sin\theta \left(kT \frac{\partial f}{\partial \theta} - Mf \right) \right] \tag{2.17}$$

where ζ, k, T and M are a friction constant, Boltzmann constant, absolute temperature and torque acting on the dipole moment in the external electric field ($M = -\mu F sin\theta$), respectively. When the oscillating external electric field is applied, the distribution function of the dipole moment is obtained by solving equation 2.17.

$$f = A \left(1 + \frac{1}{1 - i\omega\tau'} \frac{\mu F cos\theta}{kT} \right) \tag{2.18}$$

where μ is permanent dipole moment and τ' is microscopic relaxation time ($\tau' = \frac{\zeta}{2kT}$). Using the distribution function, the average orientation polarization of polar molecules can be calculated as follows,

$$P_{orient} = N\mu < cos\theta >= N\mu \frac{\int cos\theta \cdot f d\Omega}{\int f d\Omega} = \frac{N\mu^2 F}{3kT(1 - i\omega\tau')} \tag{2.19}$$

Now, using the definition of polarization, we get

$$P(\omega) = \varepsilon_0(\varepsilon(\omega) - 1)E(\omega) = N\left(\alpha F + \mu_{ave}\right) = N\left(\alpha + \frac{\mu^2}{3kT(1 - i\omega\tau')}\right)\left(\frac{\varepsilon(\omega)+2}{3}\right)E(\omega) \tag{2.20}$$

where α is polarizability and for the local electric field Lorentz field was used ($F = \frac{\varepsilon+2}{3}E$). When equation 2.20 is rearranged with respect to the dielectric constant, we get the key equation, i.e., Clausius-Mosotti relation as follows,

$$\frac{\varepsilon-1}{\varepsilon+2} = \frac{N}{3\varepsilon_0}\left(\alpha + \frac{\mu^2}{3kT(1-i\omega\tau')}\right) \tag{2.21}$$

Above relation is expressed as below in the low frequency limit ($\omega\tau' \ll 1$),

$$\frac{\varepsilon-1}{\varepsilon+2} = \frac{N}{3\varepsilon_0}\left(\alpha + \frac{\mu^2}{3kT}\right) \tag{2.22}$$

and in the high frequency limit ($\omega\tau' \gg 1$),

$$\frac{\varepsilon-1}{\varepsilon+2} = \frac{N}{3\varepsilon_0}\alpha \tag{2.23}$$

When equation 2.22 and 2.23 are combined,

$$\frac{\varepsilon-1}{\varepsilon+2} = \frac{\varepsilon_\infty-1}{\varepsilon_\infty+2} + \left[\frac{\varepsilon_s-1}{\varepsilon_s+2} - \frac{\varepsilon_\infty-1}{\varepsilon_\infty+2}\right]\frac{1}{1-i\omega\tau'} \tag{2.24}$$

Where ε_s and ε_∞ are the dielectric constant of matter at the low and high frequency limit, respectively. After rearranging above equation, we finally get the Debye relaxation model,

$$\varepsilon(\omega) = \frac{\varepsilon_s-\varepsilon_\infty}{1-i\omega\tau} + \varepsilon_\infty \tag{2.25}$$

where τ $(= \frac{\varepsilon_s+2}{\varepsilon_\infty+2}\tau')$ is macroscopic relaxation time, which is time scale it takes for polar molecules pre-aligned under an external field to rotate in a random direction after the applied field is turned off.

At the room temperature, bulk liquid water has a dominant relaxation mode near 20 GHz [2]. In the biomolecular aqueous solution, strong electrostatic interaction

between biomolecular surface and interfacial water causes slower rotational dynamics of water molecules [3-4]. Therefore, there are modes having slower relaxation time than pure water, and in this case, it can be described by multiple Debye relaxation model as follows.

$$\varepsilon(\omega) = \sum_{j=1}^{n} \frac{S_j}{1-i\omega\tau_j} + \varepsilon_\infty \tag{2.26}$$

where n is number of relaxation modes in the aqueous solution.

2.3 Dipole-Dipole Orientational Correlation

2.3.1 Kirkwood-Frohlilch Model

In 1929, P. Debye driven the relation between the dielectric constant and polar molecular parameters (permanent dipole moment, polarizability) [1]. However, the Debye model could not exactly predict the strength of dielectric constant [5], since he approximated the system as continuum medium and did not consider the local interaction with the surrounding dipole moments. In 1939 and 1958, Kirkwood and Frohlich modified the dielectric theory by considering all local interactions using concept of statistical mechanism [6].

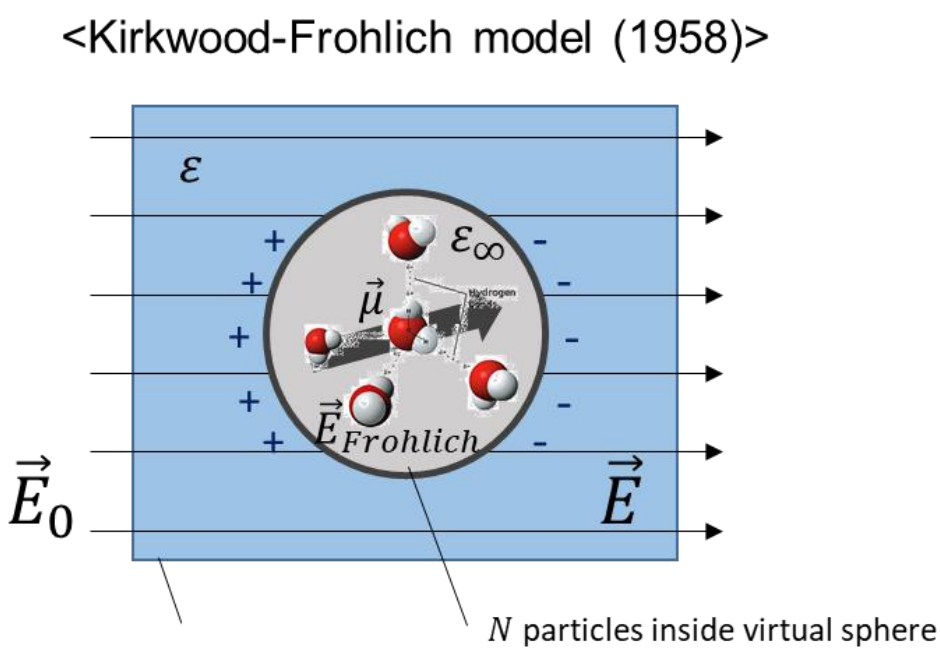

Figure 2.2. Concept of Kirkwood-Frohlich model.

They used hybrid concept, in which outside of sufficiently large sphere all water is assumed as continuum medium and inside the sphere all local interaction is considered. Polarization of the system is expressed by sum of total dipole moments,

$$P = (\varepsilon_s - 1)E = \frac{4\pi}{V}\langle \vec{M} \cdot \hat{e} \rangle \tag{2.27}$$

where $\vec{M} = \sum \vec{\mu}$ is sum of total permanent dipole moments. By using Taylor expansion, dielectric response (or dielectric constant) can be expressed in terms of external applied field, E_0,

$$\langle \vec{M} \cdot \hat{e} \rangle = \langle \vec{M} \cdot \hat{e} \rangle_0 + \left(\frac{\partial \langle \vec{M} \cdot \hat{e} \rangle}{\partial E}\right)_{E=0} E + \cdots \tag{2.28}$$

$$\varepsilon_s - 1 = \frac{4\pi}{V}\left(\frac{\partial E_0}{\partial E}\right)_{E=0}\left(\frac{\partial}{\partial E_0}\langle \vec{M} \cdot \hat{e} \rangle\right)_{E_0=0} \tag{2.29}$$

Since external field is equal to cavity field in sphere (by Gauss' law),

$$E_0 = E_c = \frac{3\varepsilon_s}{2\varepsilon_s + 1} E \tag{2.30}$$

equation 2.29 is written as

$$\varepsilon_s - 1 = \frac{4\pi}{V}\frac{3\varepsilon_s}{2\varepsilon_s + 1}\left(\frac{\partial}{\partial E_0}\langle \vec{M} \cdot \hat{e} \rangle\right)_{E_0=0} \tag{2.31}$$

A right side of equation 2.31 is derived as below when using the concept of ensemble average, $\langle \vec{M} \cdot \hat{e} \rangle = \frac{\int dX \vec{M} \cdot \hat{e} exp(-U/kT)}{\int dX exp(-U/kT)}$,

$$\left(\frac{\partial}{\partial E_0}\langle \vec{M} \cdot \hat{e} \rangle\right)_{E_0=0} = \left[\left\langle \frac{\partial \vec{M} \cdot \hat{e}}{\partial E_0} \right\rangle_0 - \frac{1}{kT}\left\langle \vec{M} \cdot \hat{e}\, \frac{\partial U}{\partial E_0} \right\rangle_0\right] \tag{2.32}$$

By considering all electrical energy in the system, above equation can summarized as [6],

$$\varepsilon_s - 1 = \frac{4\pi}{V}\frac{3\varepsilon_s}{2\varepsilon_s + 1}\frac{\langle M^2 \rangle_0}{3kT} \tag{2.33}$$

$\langle M^2 \rangle_0$ can be calculated by considering all local interaction (U) from statistical approach,

$$\langle M^2 \rangle_0 = \sum_{i=1}^{N} \frac{\int dX^N \vec{\mu}_i \cdot \vec{M} exp(-\boldsymbol{U}/kT)}{\int dX^N exp(-\boldsymbol{U}/kT)} = N\mu^2 \sum_{j=1}^{N} \int \frac{\int dX^{N-i} cos\theta_{ij} exp(-\boldsymbol{U}/kT)}{\int dX^N exp(-\boldsymbol{U}/kT)} dX^i =$$
$$N\mu^2 \sum_{j=1}^{N} \langle cos\theta_{ij} \rangle \equiv N\mu^2 g_K \quad (2.34)$$

where g_K $(= \langle \sum_j^N \hat{\mu} \cdot \hat{\mu}_j \rangle)$ is Kirkwood correlation factor which represent intermolecular dipole-dipole orientation correlation. When equation 2.34 is inserted into equation 2.33, Kirkwood-Frohlich equation is finally derived,

$$\mathrm{S} = \varepsilon_s - \varepsilon_\infty = \frac{g_K N\mu^2}{9k_B T\varepsilon_0} \frac{\varepsilon_s(\varepsilon_\infty+2)^2}{(2\varepsilon_s+\varepsilon_\infty)} \quad (2.35)$$

where S is the dielectric strength of the relaxation mode.

2.3.2 Kivelson-Madden Model

Relaxation phenomena of collective dipolar ensemble and single particle can be described by introducing the total ($C_{coll}(t)$) and self correlation function ($C_{sp}(t)$), respectively.

$$C_{coll}(t) = \langle \vec{M}(0) \cdot \vec{M}(t) \rangle \quad (2.36)$$
$$C_{sp}(t) = \langle \vec{\mu}(0) \cdot \vec{\mu}(t) \rangle \quad (2.37)$$

Then, relaxation times of collective and single particular are defined as follow,

$$\tau_{coll} = -C_{coll}(t)/[dC_{coll}(t)/dt] \quad (2.38)$$
$$\tau_{sp} = -C_{sp}(t)/[dC_{sp}(t)/dt] \quad (2.39)$$

By assuming mono correlation time and initial condition of correlation function,

($C_{coll}(t) = exp(-t/\tau_{coll}),\ C_{sp}(t) = exp\left(-t/\tau_{sp}\right),\ C_{coll}(0) = C_{sp}(0) = 1$)), we can derive as,

$$\tau_{coll} = \tau_{sp} \cdot \gamma(0) \Big/ \left[1 + \frac{d\gamma(t)/dt}{dC_{sp}(t)/dt}\right] \tag{2.40}$$

where $\gamma(t)(= 1 + \langle \vec{\mu}_i(0) \sum_j^N \vec{\mu}_j(t) \rangle / \langle \mu^2(0) \rangle)$ is cross-correlation function. When cross-correlation ($\gamma(t)$) decays substantially slower than single-correlation ($C_{sp}(t)$) decay,

$$\tau_{coll} \approx \gamma(0) \cdot \tau_{sp} = g_K \tau_{sp} \tag{2.41}$$

where $g_K(= \sum_{j=1}^N \langle \hat{\mu}_i(0) \cdot \hat{\mu}_j(0) \rangle)$ is Kirkwood correlation factor. Above Kivelson-Madden equation (2.41) suggests that from the macroscopic measurement of collective relaxation time of polar liquids, the intermolecular orientation correlation (g_K) can be investigated.

2.4 Effective Medium Theory

2.4.1 Overview

Effective medium theory describes averaged dielectric properties of system from distinct all components.

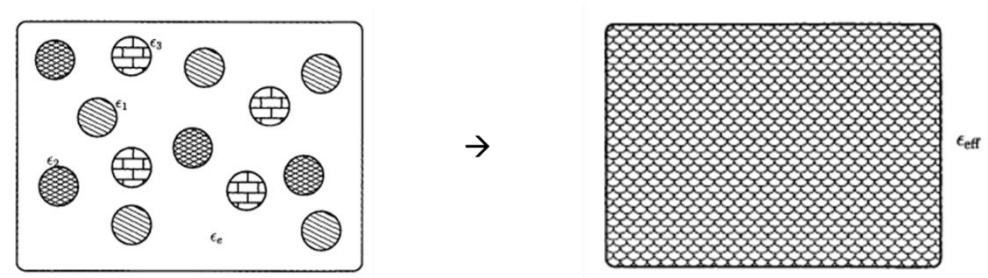

$$\epsilon_1 + \epsilon_2 + \epsilon_3 + \cdots \rightarrow \epsilon_{eff}$$

Figure 2.3. Concept of effective medium theory.

There are lots of effective medium models and each has own limitation. The Bruggeman mixture model is most widely used in the aqueous environment since which can be applicable to high mixture concentration. Bruggeman model has been successfully used to investigate unknown dielectric information in interfacial water [7] or nanoconfined water [8].

2.4.2 Bruggeman Mixture Model

Bruggeman model can be simply derived using concept of conservation of electric flux. Total flux (D) in the system is expressed by linear sum of each components (Figure 2.4).

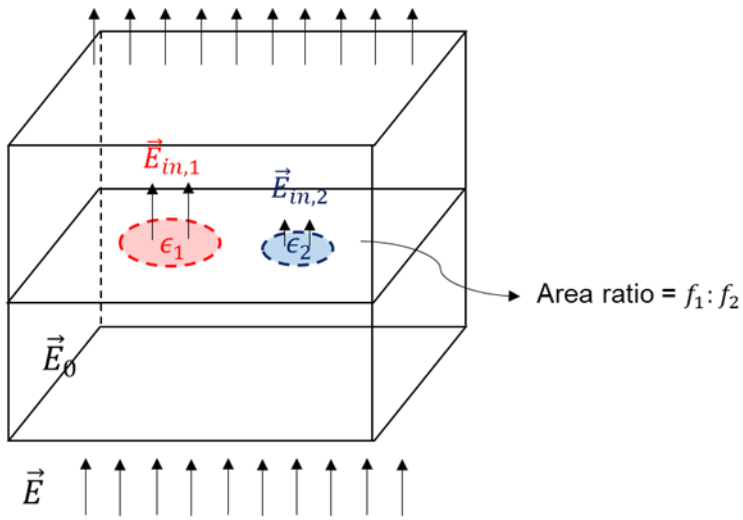

Figure 2.4. Electric flux inside the material which composed by two different components.

$$D_{eff} = f_1 D_1 + f_2 D_2 = f_1 \varepsilon_1 E_{in,1} + f_2 \varepsilon_2 E_{in,2} = \varepsilon_{eff} E_0 \tag{2.42}$$

Above equation can be rearranged as,

$$f_1\left(\varepsilon_1 E_{in,1} - \varepsilon_{eff} E_0\right) + f_2\left(f_2 \varepsilon_2 E_{in,2} - \varepsilon_{eff} E_0\right) = 0 \tag{2.43}$$

When we suppose that each dielectric component are sphere, local field inside each sphere is calculated as,

$$E_{in,1} = \frac{3\varepsilon}{\varepsilon_1 + 2\varepsilon} E_0 \tag{2.44}$$

$$E_{in,2} = \frac{3\varepsilon}{\varepsilon_2 + 2\varepsilon} E_0 \tag{2.45}$$

where ε $(= \varepsilon_{eff})$ is dielectric component of the whole system. When above two equations are inserted into equation 2.43, Bruggeman equation is finally driven,

$$f_1 \left(\frac{\varepsilon_1 - \varepsilon}{\varepsilon_1 + 2\varepsilon}\right) + f_2 \left(\frac{\varepsilon_2 - \varepsilon}{\varepsilon_2 + 2\varepsilon}\right) = 0 \tag{2.46}$$

Bibliography

1. Debye, P. J. W., *Polar Molecules*. New York, The Chemical Caltalog Company: **1929**.
2. Buchner, R.; Barthel, J.; Stauber, J., *Chem. Phys. Lett.* **1999,** *306*, 57-63.
3. Cametti, C.; Marchetti, S.; Gambi, C. M. C.; Onori, G., *J. Phys. Chem. B* **2011,** *115* (21), 7144-7153.
4. George, D. K.; Charkhesht, A.; Hull, O. A.; Mishra, A.; Capelluto, D. G. S.; Mitchell-Koch, K. R.; Vinh, N. Q., *J. Phys. Chem. B* **2016,** *120* (41), 10757-10767.
5. Hill, N. E., *Dielectric Properties and Molecular Behaviour*. Van Nostrand Reinhold: **1969**.
6. Bottcher, C. J., *Theory of Electric Polarization, Vol.1 Dielectrics in Static Fields*. 2nd ed.; Ch. 6 Elsevier, Amsterdam: **1973**.
7. Vinh, N. Q.; Allen, S. J.; Plaxco, K. W., *J. Am. Chem. Soc.* **2011,** *133* (23), 8942-8947.
8. Choi, D.-H.; Son, H.; Jeong, J.-Y.; Park, G.-S., *Chem. Phys. Lett.* **2016,** *659*, 164-168.

Chapter 3.
Methods and Materials

3.1 Dielectric Relaxation Spectroscopy (DRS)

3.1.1 Overview

Dielectric relaxation spectroscopy measures dielectric response of materials to external oscillating electric field. It is based on the interaction of dipole moment of sample with external field, which is expressed by complex dielectric constant (Dispersion and energy loss). There are different kinds of field-matter interactions depending on the field frequency (Figure 3.1).

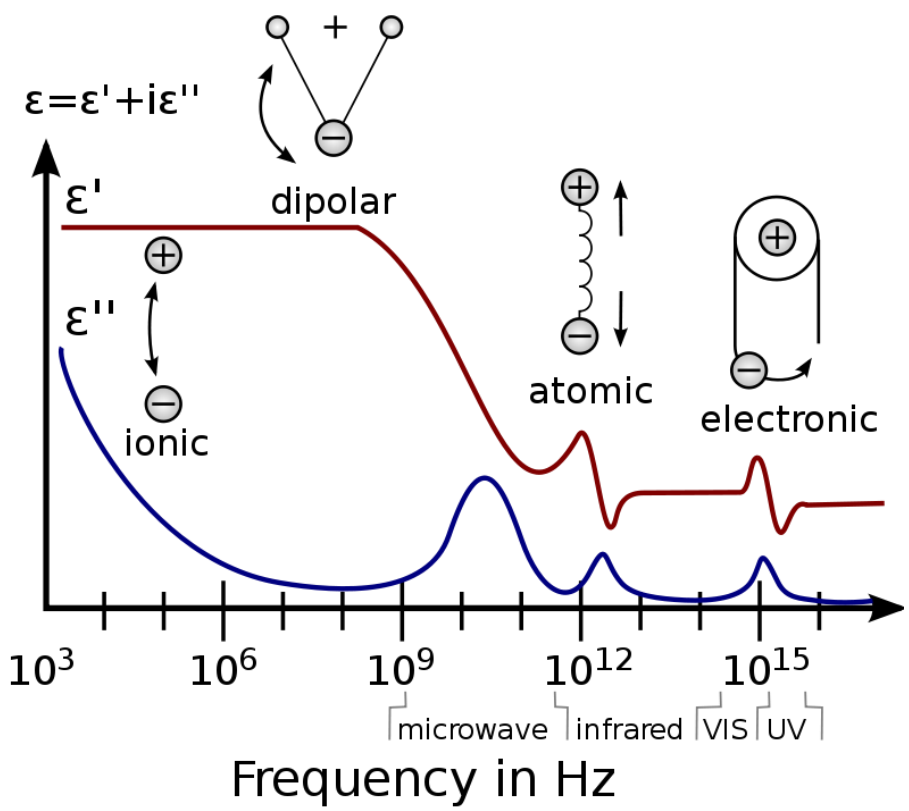

Figure 3.1. Frequency response of dielectric polarization of typical polar liquids [1].

The strength of the dielectric constant is dominantly determined by the collective reorientation response of water dipoles to the applied field (about 92% [2]), which exists in the GHz and is called “relaxation mode” as described in Chapter 2.2. This inherent ability to probe “collective motion” of water molecules makes dielectric relaxation spectroscopy (DRS) a special tool to investigate the intermolecular orientation correlation (or Kirkwood factor, g_K). Since water has strongly associated structure (through hydrogen bonds), water dipoles have correlated reorientation motion, which effectively enhances the dielectric constant. Therefore, to study the molecular mechanism of how NaCl changes the dielectric constant of nanoconfined water, it is helpful to investigate the change of the orientation correlation factor (g_K) using GHz DRS.

3.1.2 Open-Ended Coaxial Probe Method

Most widely used and easy method for measuring dielectric constant of polar liquids in GHz region is open-ended coaxial probe method (Figure 3.2). This method can measure the dielectric constant over a wide frequency range, and sample preparation is simple because a closed sample cell system is not needed. Generally, the reflection coefficient from the probe-sample interface is measured by a vector network analyzer (VNA) in open-ended coaxial probe method (Figure 3.3). The VNA usually consists of two or more ports and is a device that measures reflection or transmission coefficient (Figure 3.4). Scattering matrix is

$$\begin{pmatrix} b_1 \\ b_2 \end{pmatrix} = \begin{pmatrix} S_{11} & S_{12} \\ S_{21} & S_{22} \end{pmatrix} \begin{pmatrix} a_1 \\ a_2 \end{pmatrix} \tag{3.1}$$

The transmission (S_{ij}) and reflection coefficient (S_{ii}) is as below, respectively

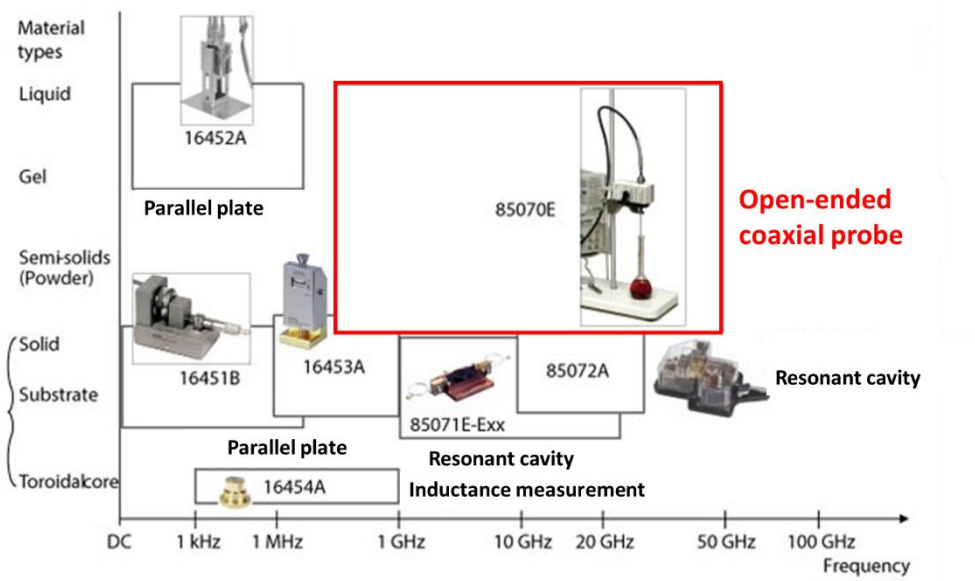

Figure 3.2. Various methods for measuring the dielectric constant of different kinds of samples over a wide frequency range

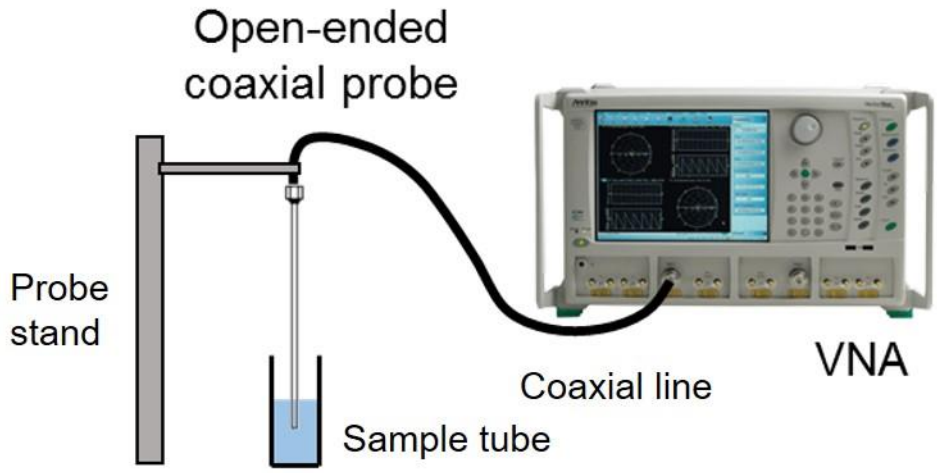

Figure 3.3. Schematics of reflection coefficient measurement using open-ended coaxial probe

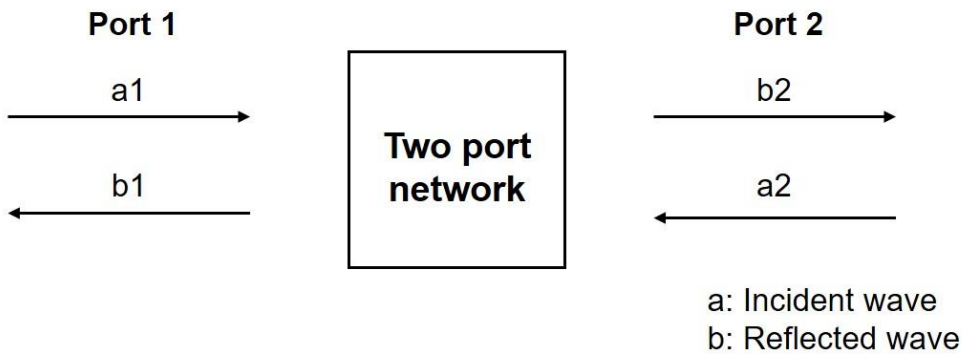

Figure 3.4. Schematics of two port network system

$$S_{12} = \frac{b_1}{a_2} = \frac{V_1^{re}}{V_2^{in}},\ S_{21} = \frac{b_2}{a_1} = \frac{V_2^{re}}{V_1^{in}} \quad (3.2)$$

$$S_{11} = \frac{b_1}{a_1} = \frac{V_1^{re}}{V_1^{in}},\ S_{22} = \frac{b_2}{a_2} = \frac{V_2^{re}}{V_2^{in}} \quad (3.3)$$

where V^{in} and V^{re} are incident and reflected voltage waves, respectively. There are no analytical method for calculation of dielectric constant from measured reflection coefficient. Therefore, several approximate models have been developed

to probe the dielectric constant.

3.1.3 Bilinear Model

The main problem of open-ended coaxial method is there is no analytical way to obtain dielectric constant from measured reflection coefficient. Therefore, in this thesis one of widely used approximate model, called "bilinear model" was used [3],

$$\varepsilon_s(\omega) = \frac{A(\omega)\rho(\omega)+C(\omega)}{1+B(\omega)\rho(\omega)} \tag{3.4}$$

where ε_s, ρ and ω are dielectric constant of sample, reflection coefficient at the calibration plane and angular frequency, respectively. A, B and C are frequency dependent coefficients that relates the reflection coefficient and dielectric constant of sample. The main assumption of this method is that the probe-sample interface can be expressed as an equivalent circuit composed by two capacitors (Figure 3.5). The derivation of the formula (3.4) is as below.

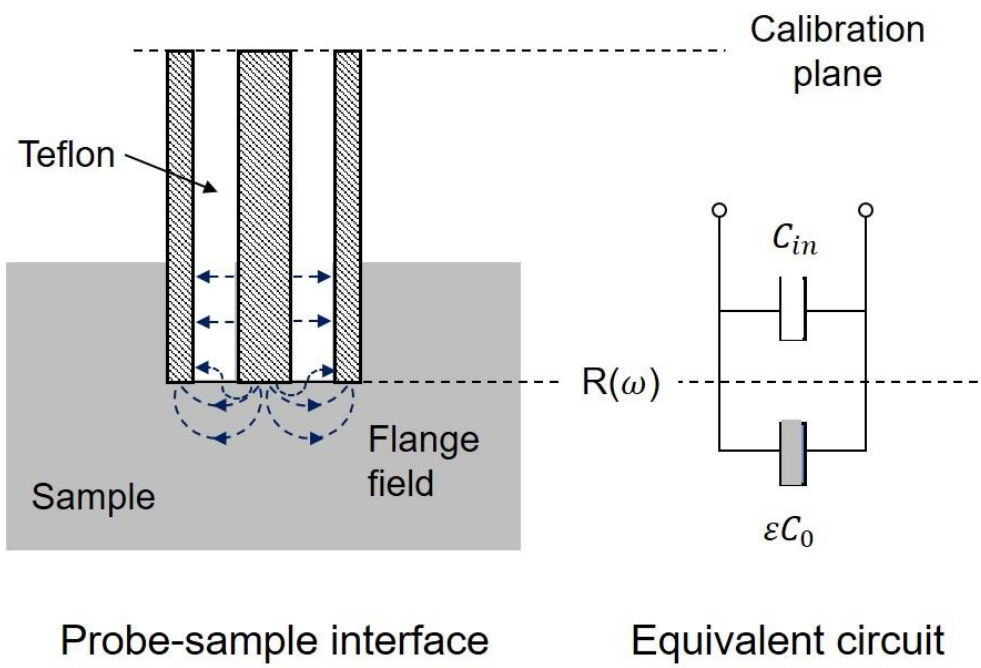

Figure 3.5. Schematics of equivalent circuit of probe-sample interface

We can calculate admittance (Y) at the probe-sample interface in two different ways. (i) The first method is to express Y on the actual device, i.e., transmission line,

$$Y = \frac{I}{V} = \frac{G_c(V^{in} - V^{re})}{(V^{in} + V^{re})} = \frac{G_c(\Gamma - 1)}{(\Gamma + 1)} \tag{3.5}$$

where V and I are voltage and current at the interface. G_c and Γ $(= V^{re}/V^{in})$ are the characteristic admittance of coaxial probe and reflection coefficient at the probe-sample interface, respectively.

(ii) The second way is to express Y on the equivalent circuit consisting of two capacitors,

$$Y = j\omega(C_{in} + \varepsilon_s C_0) \tag{3.6}$$

where j, C_{in} and C_0 are the imaginary number, capacitance inside coaxial probe and at interface, respectively. Then two equations (3.5 and 3.6) are combined to relate ε_s to reflection coefficient (ρ),

$$\varepsilon_s = \left(\frac{G_c}{j\omega C_0}\right)\frac{1-\Gamma}{1+\Gamma} - \frac{C_{in}}{C_0} \tag{3.7}$$

Finally, we replace Γ to measurable parameter, i.e., reflection coefficient (ρ) at the calibration plane (Figure 3.6),

$$\Gamma = \frac{a_2}{b_2} = \frac{A'\rho + B'}{C'\rho + 1} \tag{3.8}$$

where *A'*, *B'* and *C'* are coefficients.

$$\varepsilon_s = \frac{A\rho + C}{1 + B\rho} \tag{3.4}$$

To complete above bilinear formula, we need to determine three unknown

parameters *A*, *B* and *C*. In this thesis, we used well-known dielectric constant of three materials (in this study: air, water, 2 propanol) and

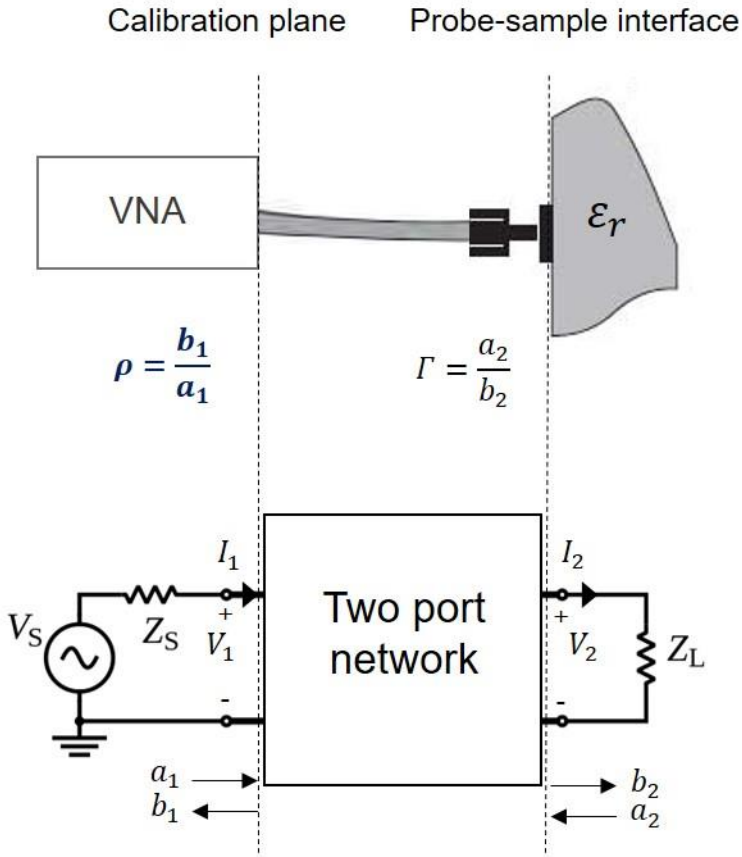

Figure 3.6. Equivalent circuit with scattering matrix

measured reflection coefficient (ρ) and bilinear formula was determined.

3.1.4 Experimental Setup

Total complex dielectric constant, $\eta^*(\nu)$, of liquid solutions were measured over the frequency range of 0.1 GHz to 70 GHz using a vector network analyzer (VNA) (ME7838A, Anritsu Inc.) with an open-ended coaxial probe (85070E, Keysight Inc.) (Figure 3.7). The bilinear model (equation 3.4) was used to determine complex dielectric constants from the measured complex reflection coefficient $\Gamma^*(\nu)$ [3]. The total complex dielectric constant, η^*, is a sum of the dielectric constant of the sample and ionic-conductivity term,

$$\eta^*(\nu) = \varepsilon^*(\nu) + \frac{i\kappa(c)}{2\pi\nu\varepsilon_0} \tag{3.5}$$

where κ is the dc ionic conductivity and ε_0 is vacuum permittivity. Conductivity, κ, of the sample was measured (Chapter3.3) to obtain dielectric constant of the sample, $\varepsilon^*(\nu)$ $(= \varepsilon'(\nu) + i\varepsilon''(\nu))$, from measured $\eta^*(\nu)$. The measurement was performed at the 303 K using the heat block (Finepcr ALB 6400) to keep the lipid phase in a fluid state at all NaCl concentration [4] since the lipid phase significantly affect surrounding water structure and dynamics [5].

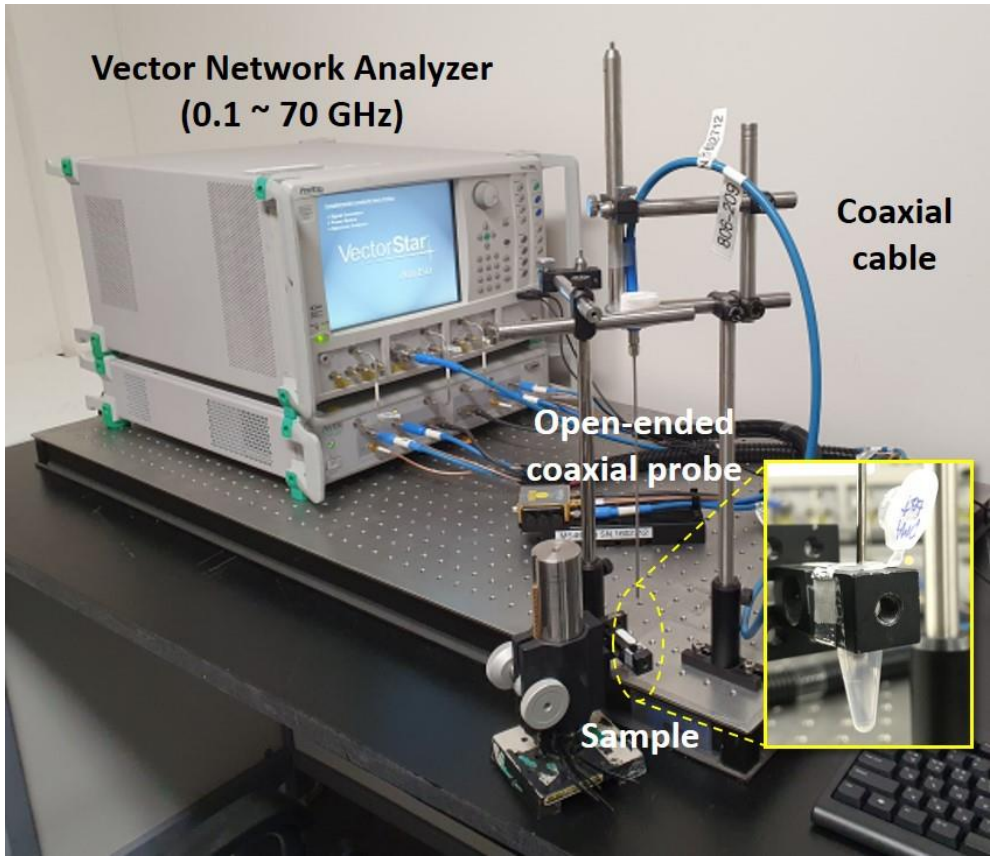

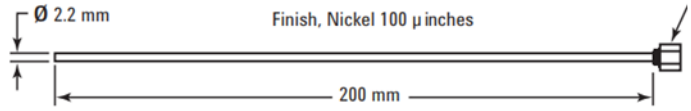

Figure 3.7. Open-ended coaxial probe connected to vector network analyzer for 0.1-70 GHz dielectric measurement

3.2 Small Angle X-ray Scattering (SAXS)

3.2.1 Principle

Small angle X-ray scattering (SAXS) is a technique that measures internal repeat nano structure of sample in solution. When there is a periodic nano structure inside the sample, the scattering intensity enhanced by constructive interference at a specific angle (θ') is detected, which is called Bragg's law (Figure 3.8),

$$2dsin\theta = n\lambda \tag{3.5}$$

where d, n, θ and λ are the spacing of the crystal layers, an integer, the scattering angle and the wavelength of the X-ray, respectively.

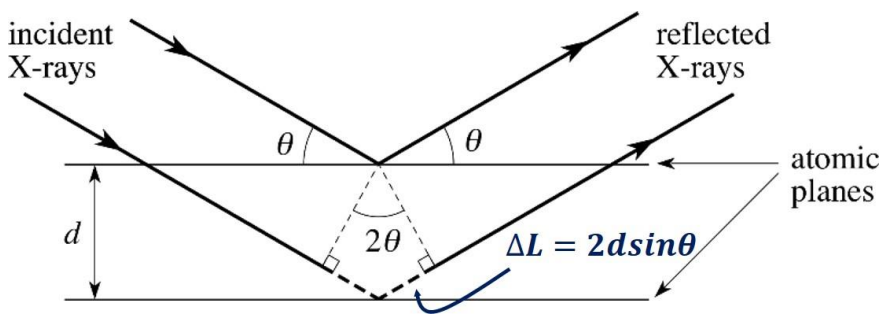

Figure 3.8. Bragg's law

When there is isotropic nano structure inside lipid vesicles dissolved in an aqueous solution, SAXS can measure lamellar repeat distance (d) from scattering vector (Δq) of the Bragg diffraction peak (Figure 3.9),

$$d = \frac{2\pi n}{\Delta q} \tag{3.6}$$

The wavelength of the X-rays typically used is 1.54 Å, and the scattered X-rays is detected by a 2D CCD camera. After averaging

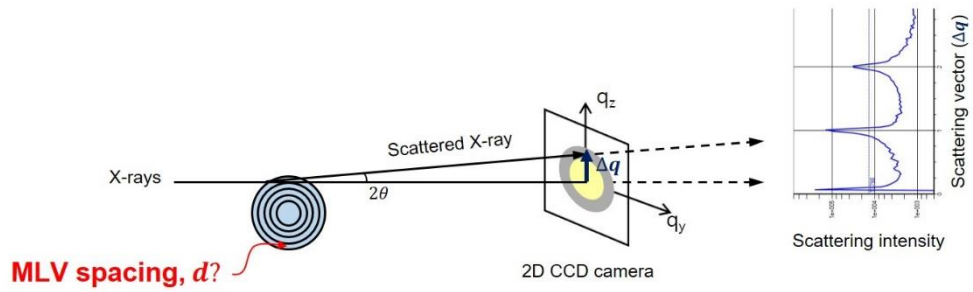

Figure 3.9. Schematics of SAXS measurement on lamellar repeat distance in lipid vesicle

the scattering intensity along the horizontal axis, we obtained the 1D graph of the scattering vector vs. scattering intensity. In order to increase the resolution of the scattering angle, the longer the sample to detector distance (SDD) is, the better because the size of CCD pixel is fixed. However, the longer the SSD is, the weaker the scattering signal is. In particular, since the intensity of the x-ray beam is weaker than that of the accelerator equipment, the commercial equipment has this disadvantage. To overcome such a limitation, a line beam method rather than a point beam is sometimes used (Figure 3.10). The SAXS device (SAXSpace, Anton-Paar Inc.) used in this thesis adopts the line beam method.

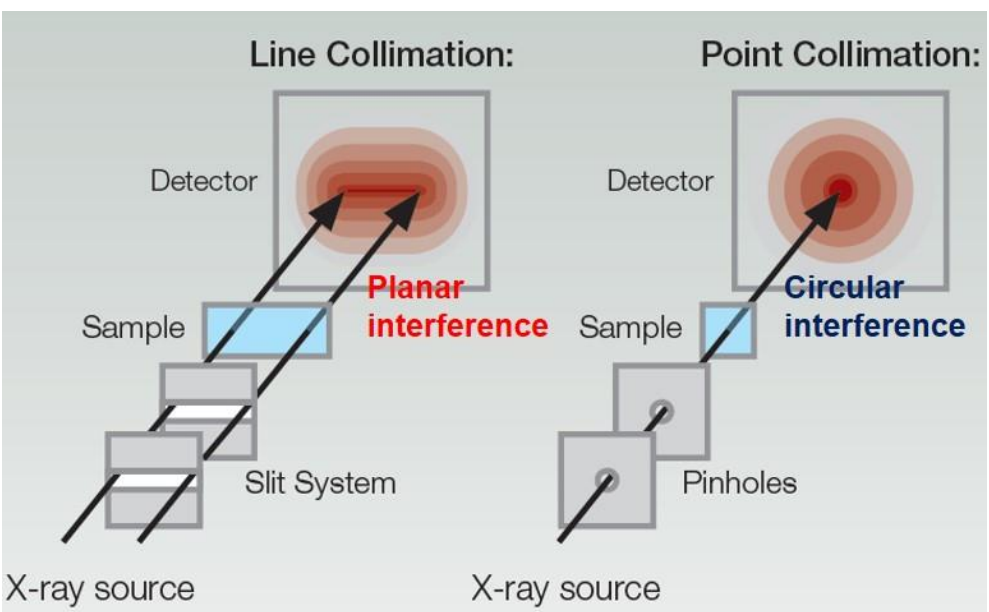

Figure 3.10. Two types of X-ray beam for SAXS measurement [6]

3.2.2 Experimental Setup

To check the existence of nano space inside DMPC MLVs, small-angle X-ray scattering (SAXS) was performed (SAXSpace, Anton-Paar Inc. at Wonkwang University and XEUSS2.0, Xenocs Inc. at Seoul National University). The wavelength of the X-rays was 1.54 Å and the scattered X-rays were detected by a 2D CCD camera (Figure 3.11 and 3.12). The position of the sample cell was calibrated using a silver behenate reference material. After averaging the scattering intensity along the horizontal axis, we obtained the 1D graph of the scattering vector vs. scattering intensity. The repeat distance (d) is obtained from the position (q) of the Bragg diffraction peak ($q=2\pi/d$) for DMPC/NaCl solutions. The temperature of liquid sample was controlled to 303 K.

Figure 3.11. Experimental setup for SAXS (Wonkwang University)

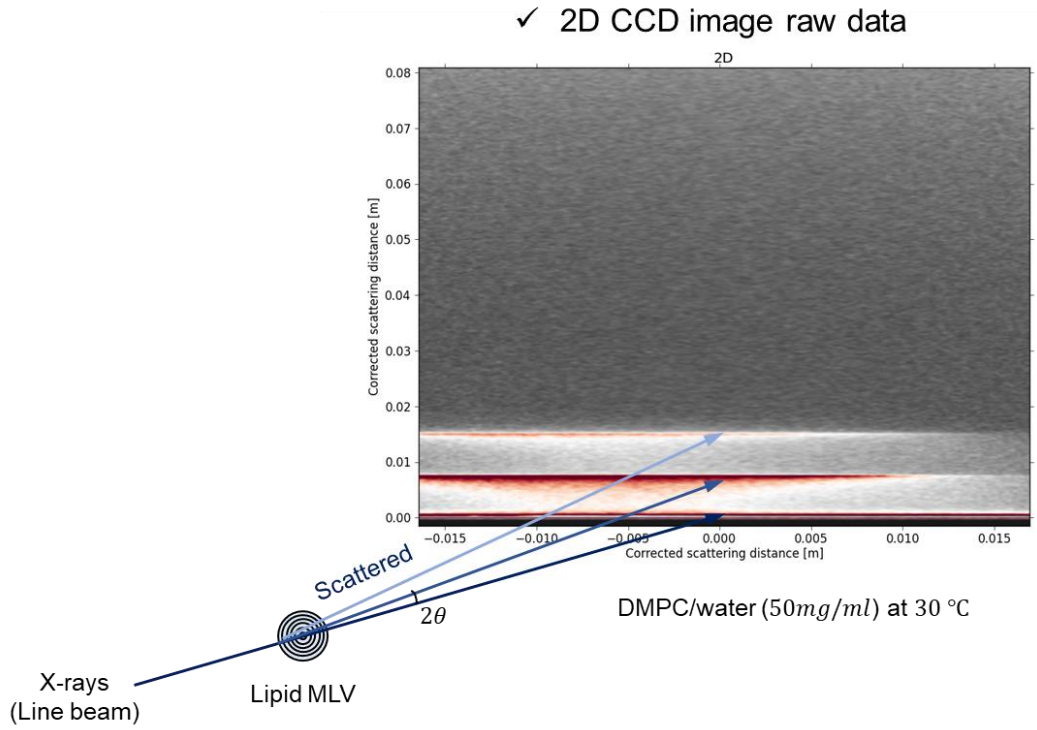

Figure 3.12. Scattered line-collimated beam from lipid MLVs is detected in 2D CCD camera

3.3 Conductivity of NaCl/Lipid Aqueous Solution

3.3.1 Principle

To analyze the dielectric constant of samples ($\varepsilon^*(\nu)$) we need to subtract ionic conductivity term from measured total dielectric constant (Chapter 5.1). Therefore, DC conductivity (κ) of solution NaCl/lipid aqueous solution was measured by conductivity meter (Figure 3.13),

$$\kappa = \vec{J}/\vec{E} \tag{3.7}$$

where $\vec{E}$ and $\vec{J}$ are bias electric field and measured current, respectively. Bias electric field is calculated from bias voltage and distance between two electrodes ($E = V/d$).

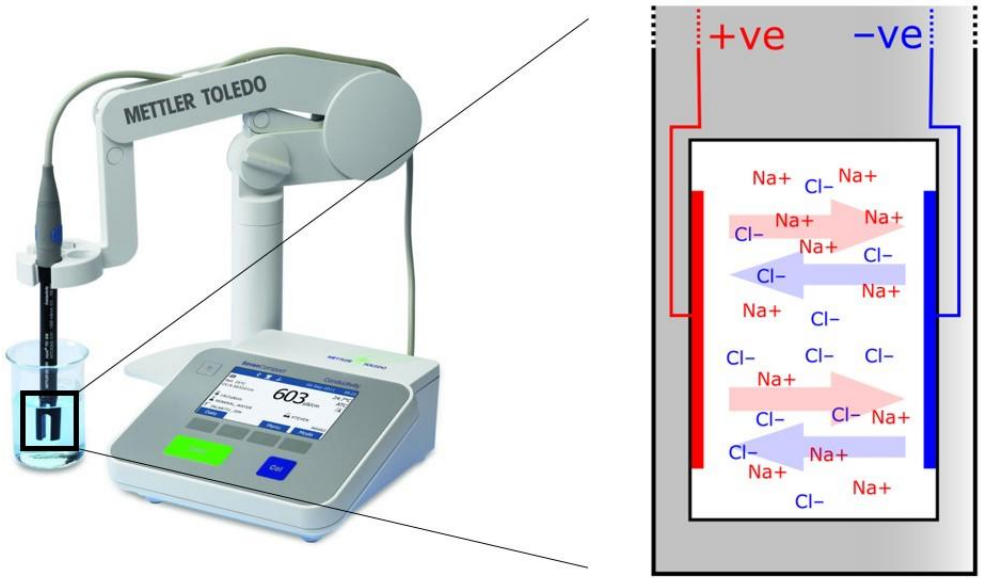

Figure 3.13. Schematics of measurement of DC conductivity of electrolyte solution

3.3.2 Experimental Setup

Conductivities, κ, of the all liquid samples were measured using conductivity meter (SevenCompact S230, Mettler Toledo Inc.) to obtain dielectric constant of the sample, $\varepsilon^*(\nu)$ $(= \varepsilon'(\nu) + i\varepsilon''(\nu))$, from measured $\eta^*(\nu)$ (equation 3.5). The conductivity meter was immersed into liquid samples in which the temperature was controlled to 303 K using heat block (Finepcr ALB 6400).

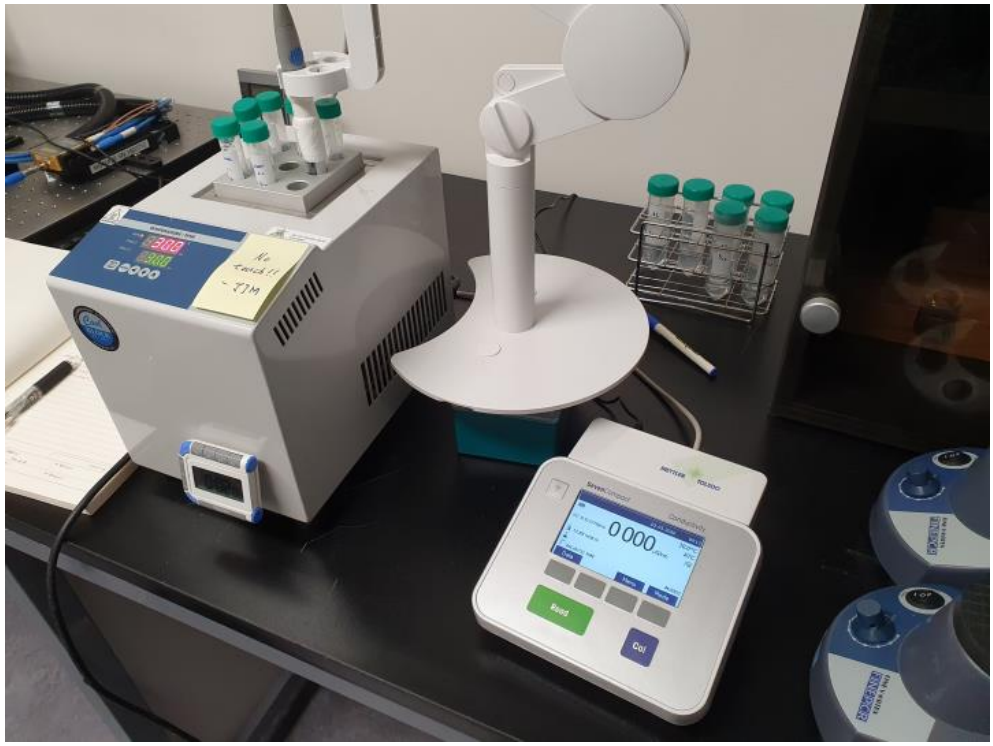

Figure 3.14. Experimental setup for ion conductivity measurement of liquid samples

3.5 Sample

3.5.1 Lipids

A lipid is any of organic compounds that is soluble in nonpolar solvents, such as fats, oils, hormones, or component of cell membranes. Some types of lipids have amphiphilic nature, in other words, one molecule has both hydrophobic and hydrophilic properties at the same time. For example, phospholipid, one of the main components of cell membrane, consist of polar head group and non-polar tails (Figure 3.15).

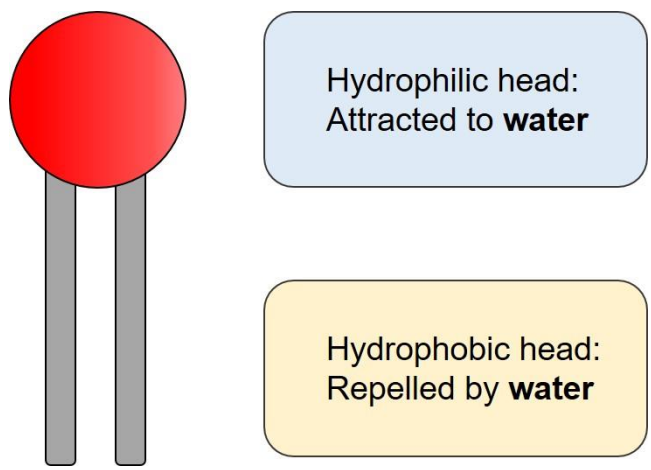

Figure 3.15. Amphiphilic property of a lipid molecule

These amphiphilic properties are essential for lipid molecules to form cell membrane structures in aqueous environment. Due to the hydrophobic effect, the non-polar tails of lipid molecules aggregate and the polar heads are exposed to water. By this "self-assembly" process, many type of structures are made such as lipid bilayer, micelle, vesicle and reverse micelle (Figure 3.16). In this thesis, phospholipid was used as an experimental platform since which is critical component in cell membrane (75% > total lipids [7]).

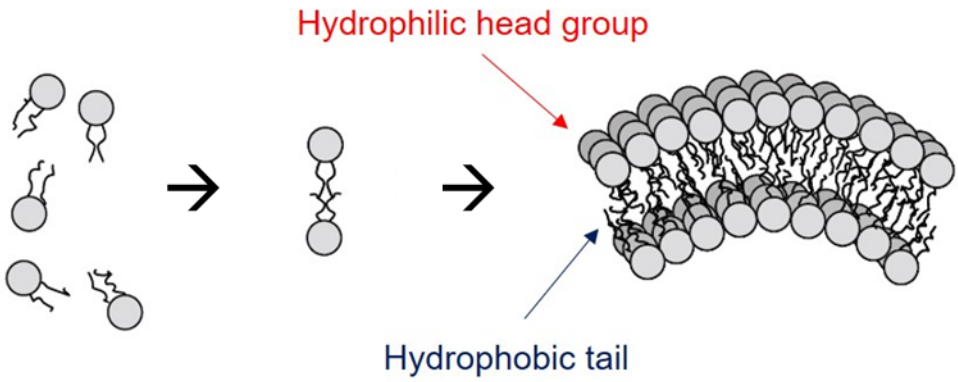

Figure 3.16. Lipid self-assembly process

3.5.2 Self-Assembly Structures

Various self-assembly structure are formed according to the structural parameters of lipid molecules. The energetically most favorable conformation is determined by the ratio of the hydrophilic/hydrophobic group size of the lipid molecule [8]. At this time, the ratio of size variables is called the packing parameter and is defined as follows,

$$P = \frac{v}{a l_c} \tag{3.8}$$

where v, a and l_c are the volume of the hydrocarbon portion, the effective area of the head group and the length of the lipid tail. Depending on the packing parameters, type of lipid self-assembly structure is determined (Figure. 3.17).

$$\begin{aligned}
&P < \tfrac{1}{3} \;\rightarrow\; \text{Spherical micelle,} \\
&\tfrac{1}{3} \leq P < \tfrac{1}{2} \;\rightarrow\; \text{Cylindrical micelle,} \\
&\tfrac{1}{2} \leq \mathrm{P} < 1 \;\rightarrow\; \text{Flexible bilayers, vesicles,} \\
&P = 1 \;\rightarrow\; \text{Planer bilayers,} \\
&P > 1 \;\rightarrow\; \text{Inverted or reverse micelle.}
\end{aligned} \tag{3.7}$$

In this thesis, we used DMPC and LMPC lipid for samples. DMPC lipid ($\frac{1}{2} \leq \mathrm{P} < 1$) self-assembles to multilamellar vesicle structure and LMPC lipid ($P < \frac{1}{3}$) self-assembles to micelle structure.

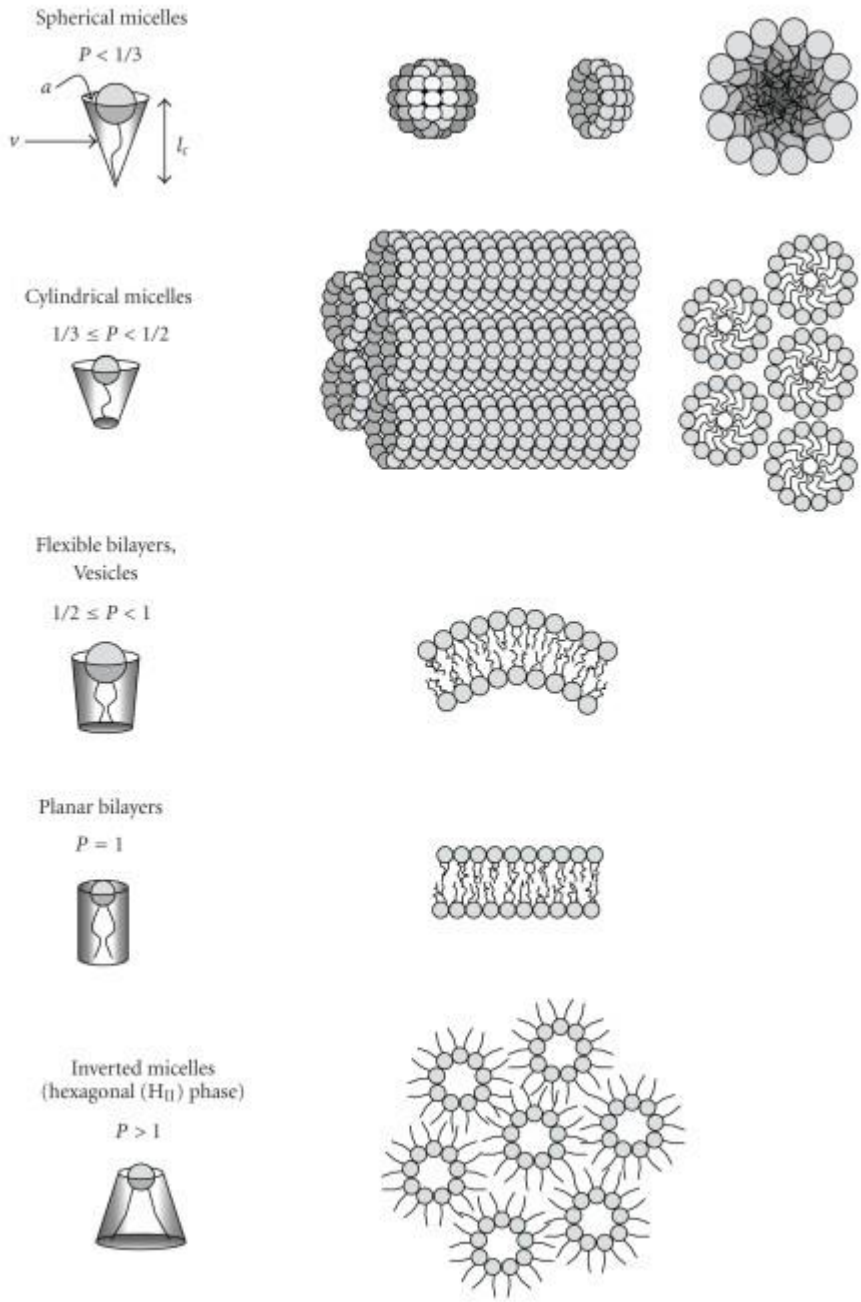

Figure 3.17. Lipid self-assembly structures depending on packing parameter [8]

3.5.3 Sample Preparation

In this thesis, phospholipid was used to mimic bio system. DMPC and LMPC were used to construct MLV (nano system) and micelle (non-nano system) as described in Chapter 3.5.2. Highly purified (>99%) synthetic 1-Myristoyl-2-Hydroxy-sn-Glycero-3-Phosphocholine (LMPC) lipid and 1,2-Dimyristoyl-sn-Glycero-3-Phosphocholine (DMPC) lipid were purchased from Anatrace, Inc. (Dussel Dr. Maumee) in powder form and used without further purification. NaCl solution (>99%) was purchased from Sigma-Aldrich (St. Louis, MO). Both LMPC and DMPC powders were dissolved in NaCl aqueous solution followed by vigorous vortex mixing. Each of NaCl aqueous solution (0, 0.1, 0.2, 0.3, 0.6, 1 M) was mixed with the lipid powders so as to achieve [mass of lipid]/[volume of NaCl solution]=150mg/1ml (Figure 3.18). Then, DMPC/NaCl solutions were cycled five times below and above the chain melting transition temperature of lipid and stored for two days at 303 K for the equilibration of ion penetration into MLV [9].

Figure 3.18. Sample preparation of lipid/NaCl solution

Bibliography

1. https://en.wikipedia.org/wiki/Dielectric_spectroscopy.
2. Buchner, R.; Barthel, J.; Stauber, J., *Chem. Phys. Lett.* **1999,** *306*, 57-63.
3. Kaatze, U., *Meas. Sci. Technol.* **2007,** *18*, 967–976.
4. Choi, D.-H.; Son, H.; Jeong, J.-Y.; Park, G.-S., *Chem. Phys. Lett.* **2016,** *659*, 164-168.
5. Choi, D.-H.; Son, H.; Jung, S.; Park, J.; Park, W.-Y.; Kwon, O. S.; Park, G.-S., *J. Chem. Phys.* **2012,** *137* (17), 175101.
6. www.anton-paar.com/.
7. Vance, J. E., *Traffic* **2015,** *16* (1), 1-18.
8. Balazs, D. A.; Godbey, W., *J Drug Deliv* **2011,** *2011*, 326497.
9. Petrache, H. I.; Tristram-Nagle, S.; Harries, D.; Kučerka, N.; Nagle, J. F.; Parsegian, V. A., *J. Lipid Res.* **2006,** *47* (2), 302-309.

Chapter 4.
Observation of Nano Space inside Lipid Multilamellar Vesicle (MLV)

4.1 MLV Repeat Distance of DMPC/NaCl solution

In this thesis, DMPC lipid was used as a platform to confine water molecules inside. It is well known that a lipid multilemaller vesicle (MLV) with a nano space inside is formed through sample preparation described in Chapter 3.5.3. We confirmed the existence of the inner nano space by measuring the lamellar repeat distance of DMPC MLV by using SAXS.

Figure 4.1 represents the graph of scattering vector vs. scattering intensity of DMPC/NaCl solutions for various NaCl concentrations.

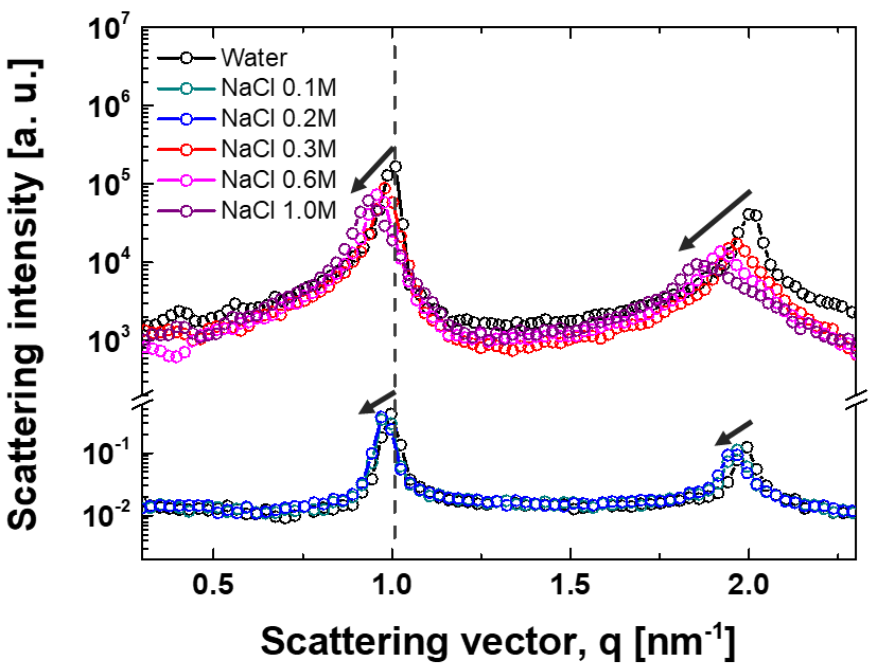

Figure 4.1. Scattering vector vs. scattering intensity for DMPC/NaCl solutions

First and second order Bragg peak was detected. Two groups of graphs (above and below) shows different intensity because two difference SAXS devices were used in this thesis. For low NaCl concentrations ($0, 0.1, 0.2\ M$), XEUSS 2.0 (Xenocs Inc. at Seoul National University) was used. For high NaCl concentrations ($0, 0.3, 0.6, 1\ M$), SAXSpace (Anton-Paar Inc. at Wonkwang University) was used. Since two different devices show almost identical Bragg diffraction peak for DMPC/water sample all experimental results are considered proper. The lamellar repeat distance (d) inside DMPC MLV was obtained from the scattering vector of Bragg diffraction peak ($q = 2\pi/d$)

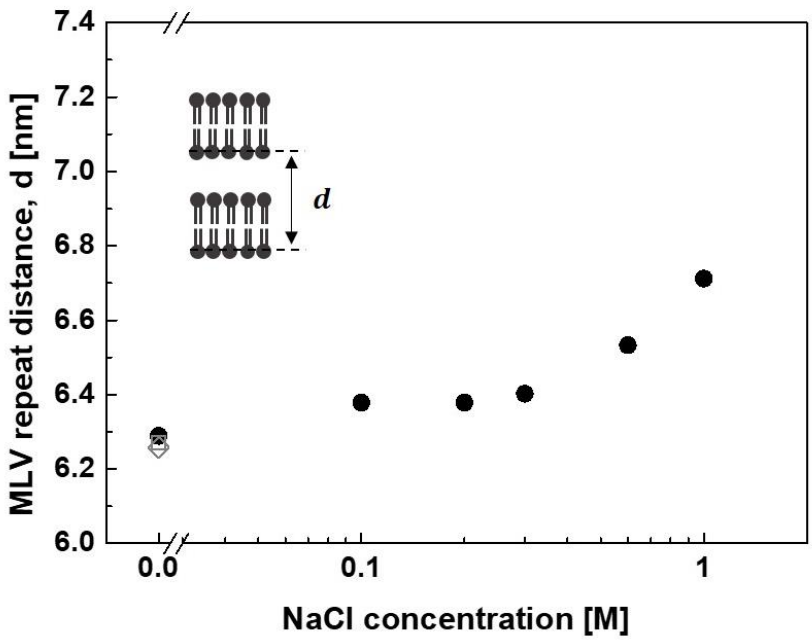

Figure 4.2. Lamellar repeat distance (d) of DMPC MLV for different NaCl concentrations

Our result is almost simillar with literature data for DMPC/water sample (gray open square [1], gry open diamond [2]). When we consider the thickness of DMPC bilayer (~4.4 nm [1]) is unaffectable by NaCl [3], the thickness of the nanoconfined water layer varies from 1.9 to 2.3 nm in MLVs. Although the water layer thickness increases by up to 22% in 1M NaCl, it has been proposed by previous simulations that the effect of the NaCl concentration change on the dielectric constant is much

stronger than that of the nano-gap change. For example, a change in the NaCl concentration from 0 to 1M induces change of the dielectric components about 20 [4], but when the nano-gap changes from 2nm to 3nm, it causes a change of less than 4 [5-7]. Therefore, DMPC MLV was considered as a useful experimental platform to probe the anomalous NaCl effect on the dielectric constant of nanoconfined water.

Bibliography

1. Nagle, J. F.; Tristram-Nagle, S., *Biochim. Biophys. Acta* **2000,** *1469* (3), 159-195.
2. Costigan, S. C.; Booth, P. J.; Templer, R. H., *Biochim. Biophys. Acta* **2000,** *1468* (1-2), 41-54.
3. Pabst, G.; Hodzic, A.; Štrancar, J.; Danner, S.; Rappolt, M.; Laggner, P., *Biophys. J.* **2007,** *93* (8), 2688-2696.
4. Jalali, H.; Lotfi, E.; Boya, R.; Neek-Amal, M., *J. Phys. Chem. B* **2021,** *125* (6), 1604-1610.
5. Fumagalli, L.; Esfandiar, A.; Fabregas, R.; Hu, S.; Ares, P.; Janardanan, A.; Yang, Q.; Radha, B.; Taniguchi, T.; Watanabe, K.; Gomila, G.; Novoselov, K. S.; Geim, A. K., *Science* **2018,** *360* (6395), 1339-1342.
6. Mondal, S.; Bagchi, B., *The Journal of Physical Chemistry Letters* **2019,** *10* (20), 6287-6292.
7. Mondal, S.; Bagchi, B., *J. Chem. Phys.* **2021,** *154* (4), 044501.

Chapter 5.
Observation of Anomalous NaCl Effect on the Dielectric Constant of Nanoconfined Water in MLVs

5.1 Obtaining Process of Dielectric Constant of All Samples

To obtain the dielectric constant ($(\varepsilon^*(\nu)$) of the sample, the ionic conductivity term ($\frac{i\kappa(c)}{2\pi\nu\varepsilon_0}$) need to be subtracted from measured total dielectric constant ($\eta^*(\nu)$) by VNA, which is well described in Chapter 2.1.2. To determine conductive loss term, we measured the conductivity of all liquid sample independently by the using conductivity meter.

Figure 5.1 represent dielectric loss (ε'') of all liquid samples.

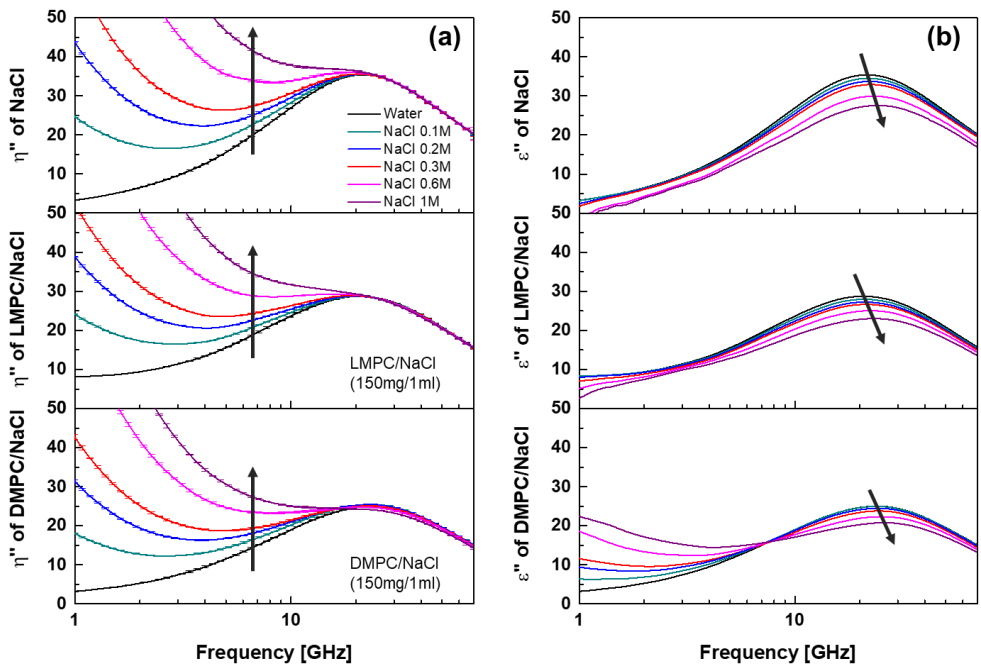

Figure 5.1. (a) Measured total dielectric loss, (b) After subtraction of ionic conductivity term from (a)

After the subtraction process, the ionic conductive loss term (shows diverge trend at

low frequency) is almost removed in both NaCl and LMPC/NaCl solution. However, in DMPC/NaCl, it is not completely removed and the reason is presumed that the part of NaCl in the sample, that is, the NaCl confined inside the MLV, is not detected by the conductivity meter measurement (Figure 5.2). In this thesis, volume fraction of MLV in the DMPC/NaCl sample is not negligible (~ 30%), which is described in Chapter 5.4, can lead to large experimental errors in the conductivity measurement can occurs.

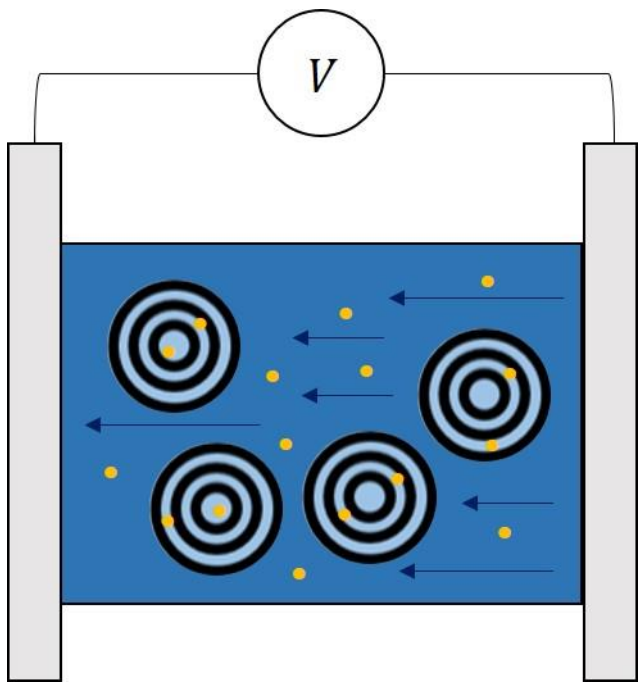

Figure 5.2. Scheme of conductivity measurement on DMPC/NaCl solution by conductivity meter

Therefore, in the case of DMPC/NaCl solution, indirect way was used for estimating the ionic conductivity term. Since this term has a dominant contribution on dielectric loss at the low frequency, we assumed that the increment of dielectric loss (ε'') at the low frequency is almost entirely due to this conductivity term, $\frac{i\kappa(c)}{2\pi\nu\varepsilon_0}$ (Figure 5.3).

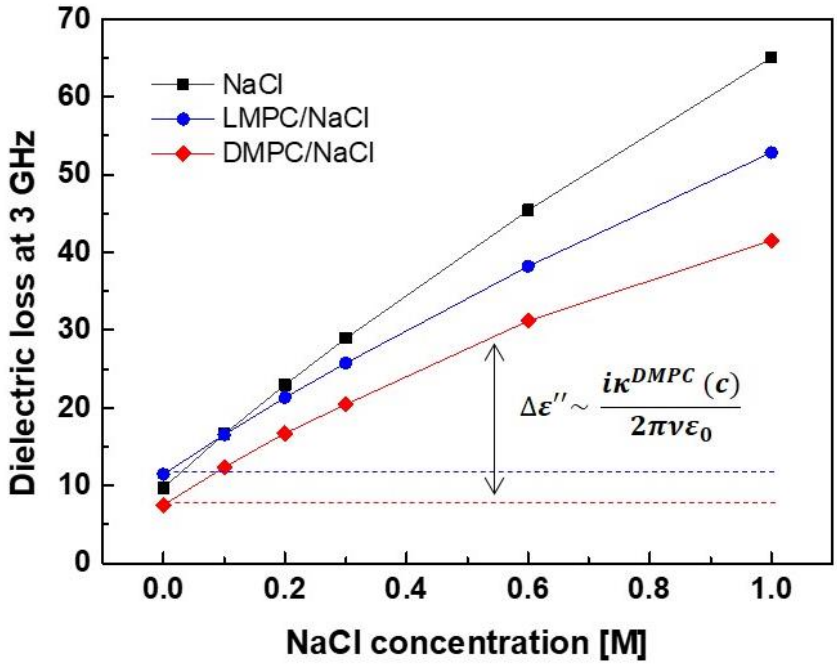

Figure 5.3. Increment of dielectric loss (ε'') at 3 GHz for all samples as a function of NaCl concentration

Then, the NaCl conductivity (κ) in DMPC/NaCl solution was finally calculated from the relationship, $\frac{[\kappa_{DMPC}]}{[\Delta\varepsilon''_{DMPC}]} = \frac{[\kappa_{LMPC}]}{[\Delta\varepsilon''_{LMPC}]}$. Calculated κ in DMPC/NaCl solution from two different frequencies (3 and 5 GHz) show almost same results and larger than measured one (Figure 5.4). After subtracting the ion conductivity term using calculated κ, finally DMPC/NaCl sample shows there is no contribution of conductivity term (Figure 5.5).

We represent final dielectric loss of all samples in Figure 5.6. We revealed the existence of the nano confinement effect on collective dynamics of water (Figure 5.6a). In the LMPC micelle and DMPC MLV, there are opposite trends and these results reproduce our group's previous observation [1]. In the LMPC solution, red shift of bulk peak was observed, which implies slower water dynamics. That is due to well-known "hydration effect", in which strong electrostatic attraction between lipid membrane surface and nearby hydration makes water molecules slow down. However, although DMPC MLV has identical surface structure as LMPC micelle, the result on bulk mode is different.

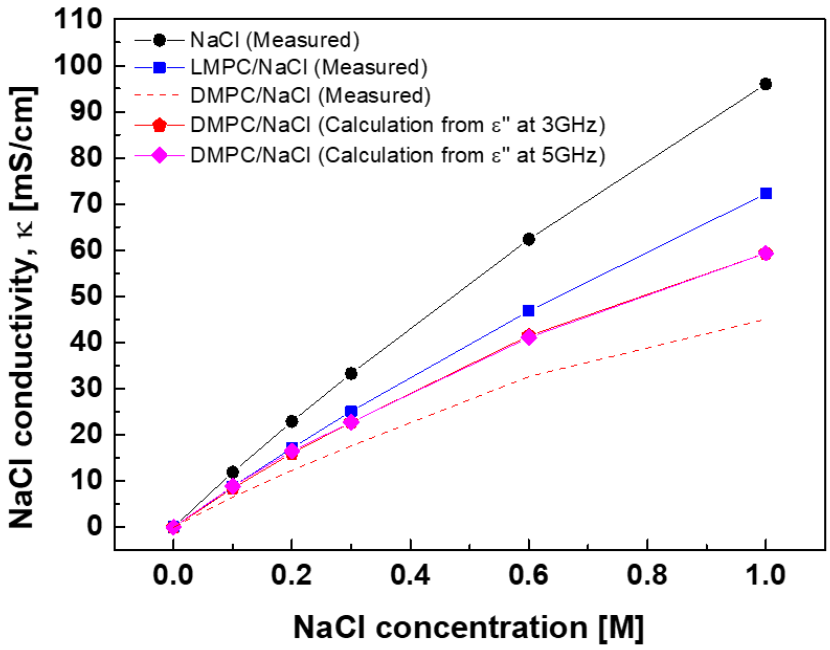

Figure 5.4. NaCl conductivity of all samples

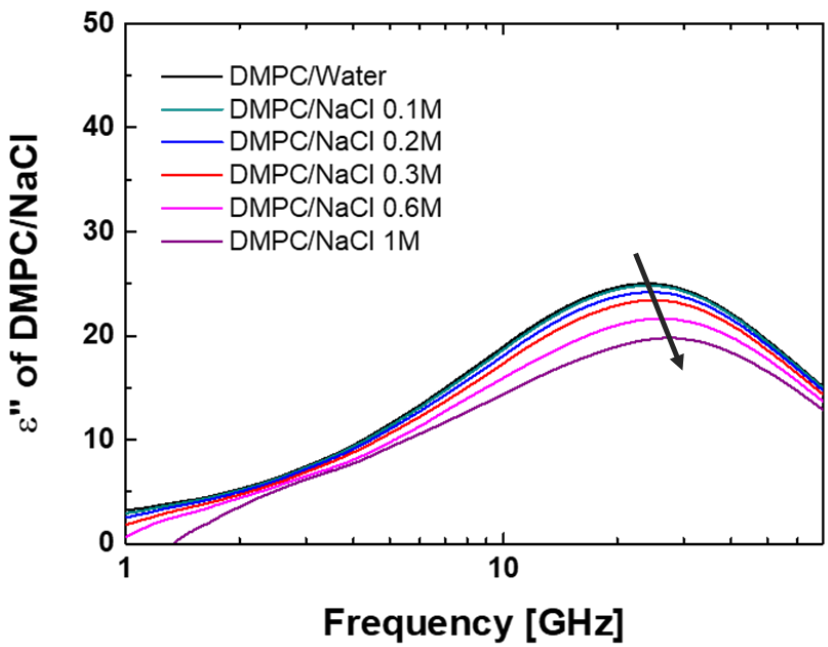

Figure 5.5. Dielectric loss of DMPC/NaCl sample after subtracting ion conductivity from measured total dielectric loss

Blue shift of bulk peak was observed, which reveals faster water dynamics. This fact suggests another effect exists than the hydration effect in nanoconfinement environment, that is, "confinement effect".

A quick scan of the NaCl effect on the dielectric loss gives two predominant observations in all samples that are systematic decrease of dielectric strength and acceleration of bulk mode peak. Further detailed analysis is in the next Chapter.

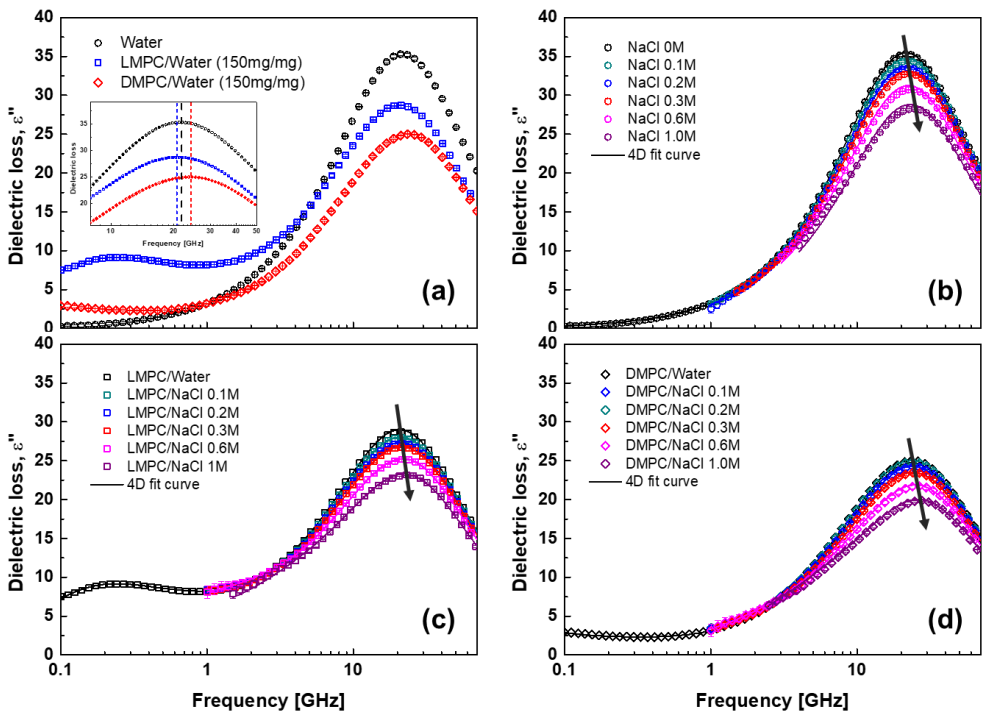

Figure 5.6. Dielectric loss (ε'') of all samples. Dielectric loss of (a) water, LMPC/water, DMPC/water, (b) NaCl, (c) LMPC/NaCl and (d) DMPC/ NaCl

The permittivity (ε') of all samples is also analyzed. Since in this real part of complex dielectric constant there is no contribution of ionic conductivity term, the permittivity was directly obtained from measured permittivity (Figure 5.7). A quick scan shows there are systematic decrease of permittivity in all samples. Detailed analysis is in the next Chapter.

In the whole samples, the dielectric data with large experimental error in low frequency region was not used.

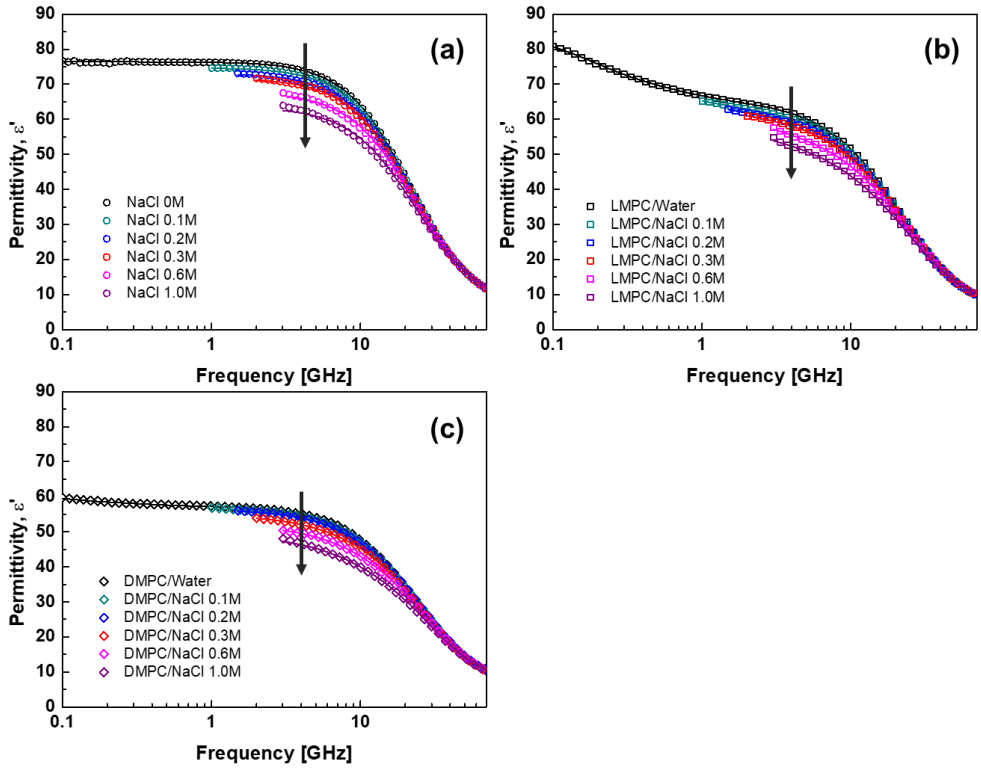

Figure 5.7. Permittivity (ε') of all samples. Permittivity of (a) NaCl, (b) LMPC/NaCl and (c) DMPC/ NaCl

5.2 Anomalous Increase of Dielectric Constant in DMPC/NaCl solution (Raw Data)

To analyze dielectric behavior in liquid samples, we simultaneously fitted permittivity (ε') and dielectric loss (ε'') of all samples. Cole-Cole relaxation model was used for NaCl solution,

$$\varepsilon^*(\nu) = \varepsilon'(\nu) + i\varepsilon''(\nu) = \frac{S}{1-(i2\pi\nu\tau)^{1-\alpha}} + \varepsilon_\infty^* \quad (5.1)$$

where α, S and τ are Cole-Cole parameter, dielectric strength and collective relaxation time of NaCl solution, respectively. For the LMPC/NaCl and DMPC/NaCl solutions, four Debye relaxation model were used,

$$\varepsilon^*(\nu) = \frac{S_s}{1-2\pi\nu\tau_s} + \frac{S_t}{1-2\pi\nu\tau_t} + \frac{S_w}{1-2\pi\nu\tau_w} + \frac{S_b}{1-2\pi\nu\tau_b} + \varepsilon_\infty^* \quad (5.2)$$

where S_s, S_t, S_w, and S_b are the dielectric strength of each Debye process for the motion of solute, tight bound, weakly bound and bulk water, respectively, whereas τ_s, τ_t, τ_w, and τ_b are there collective relaxation times of solute/NaCl solutions, respectively. Since α in NaCl solution is almost negligible (less than 0.02) in our ion concentration range, the Debye relaxation model could be applied to the bulk mode of all lipid/NaCl solutions to reduce the number of fitting parameters. For the LMPC Micelle/water, the time scale of all relaxation times ($\tau_l \sim 909 \pm 7$ ps, $\tau_t \sim 178 \pm 15$ ps, $\tau_w \sim 18 \pm 2$ ps and $\tau_b \sim 7$ ps) are in good agreement with the literature value of phospholipid micelle aqueous solution [2]. For the DMPC/NaCl solution, the relaxation time of lipid (τ_l) was held fixed at the literature value, 4000 ps [3], because the position of the mode is outside of our measurement frequency range and the NaCl almost no affects lipid bilayer structure [4-5]. Dielectric loss spectra with their mode decomposition are represented in Figure 5.8.

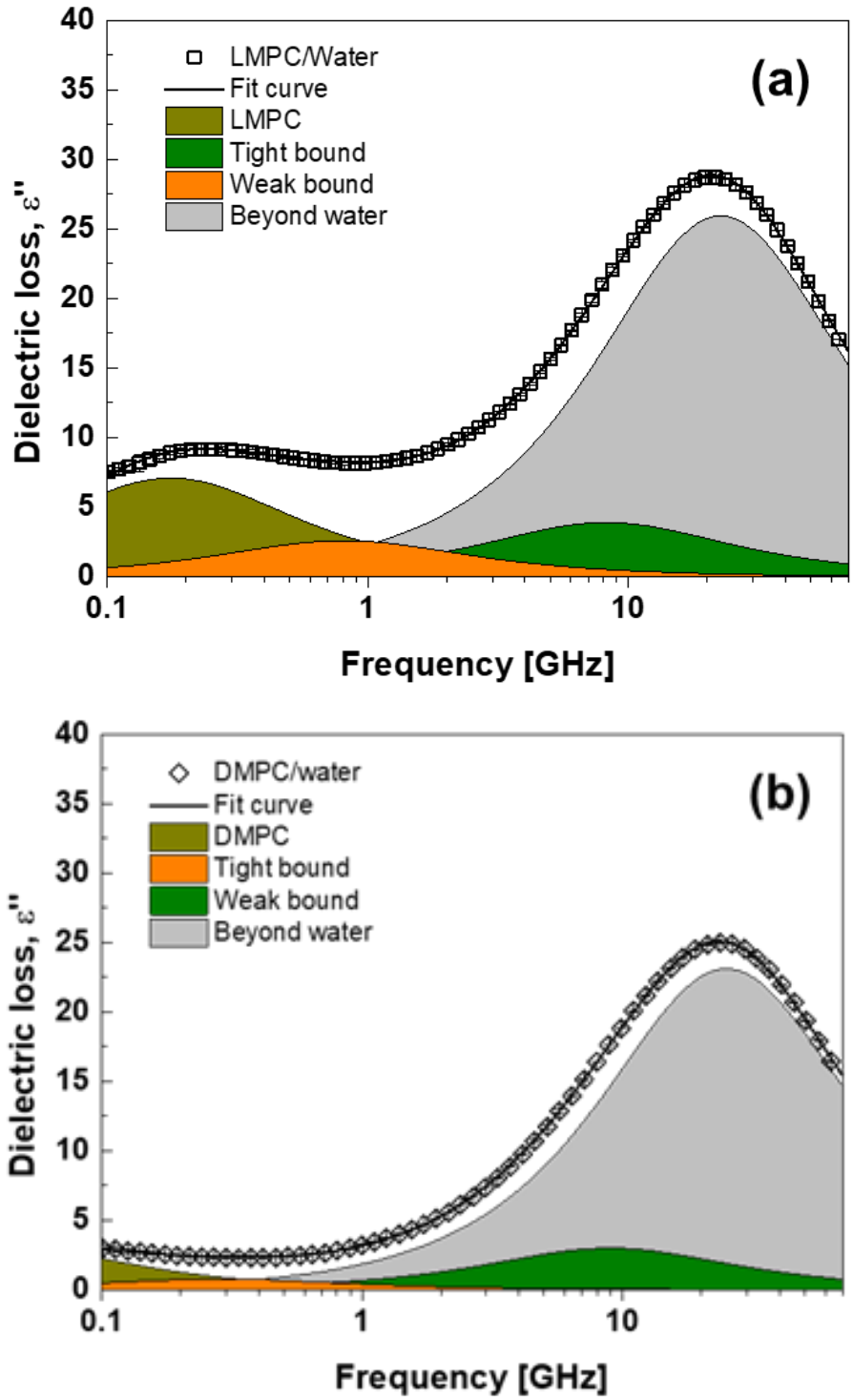

Figure 5.8. Dielectric loss spectrum, four Debye relaxation mode fit (black solid line), and their mode decomposition for (a) LMPC/water and (b) DMPC/water.

Fitting parameters of bulk mode for all samples are depicted in Figure 5.9. For the NaCl solution, simple monotonic decreases in dielectric strength and relaxation time were observed with increasing ionic concentration, the origin of which has been believed as reduced water orientation correlation (g_K) around an ion [6]. For the LMPC/NaCl solution, depolarization from ideal-bulk water amplitude is due to the hydration effect, and acceleration of τ_b compared to the NaCl solution is guessed as reduced water orientation correlation around the micellar surface. The trends of decrease of dielectric strength and relaxation time with NaCl concentration in LMPC/NaCl follow the bulk-like NaCl effect (Blue vs. black solid line).

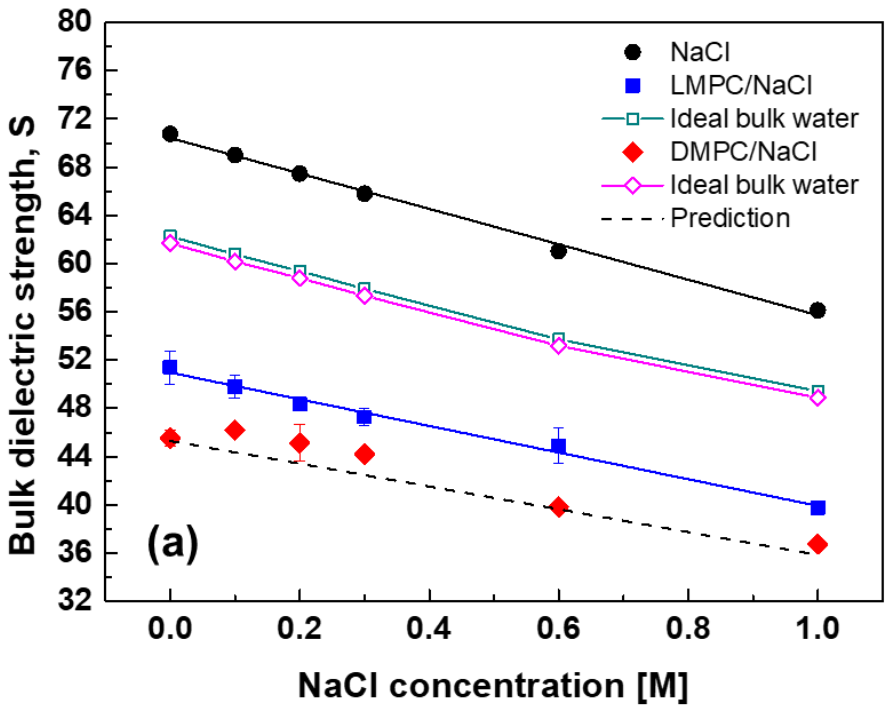

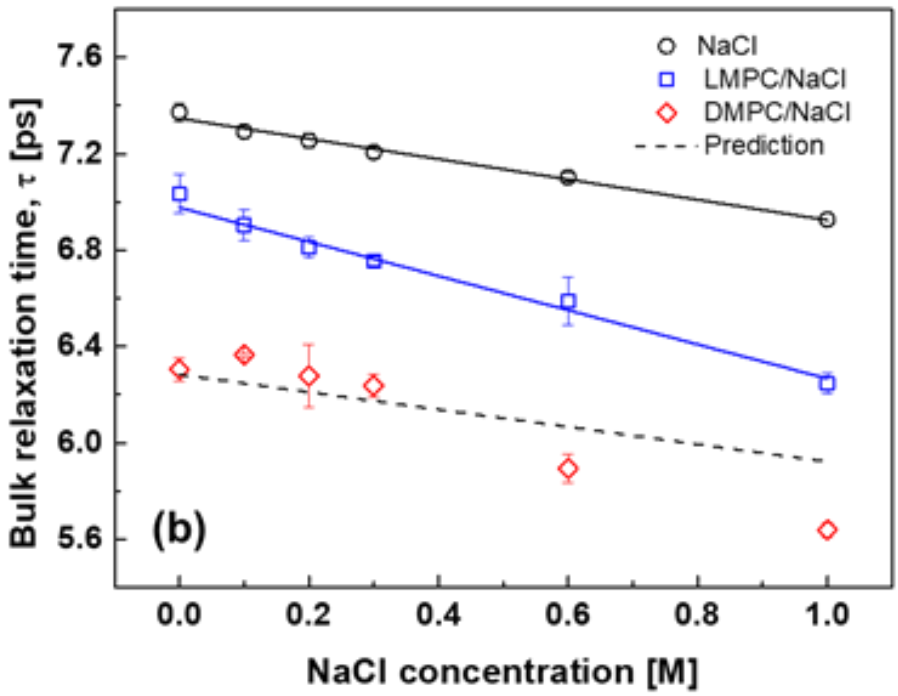

Figure 5.9. (a) Dielectric strengths and (b) relaxation times of bulk mode for all samples

On the other hand, in the DMPC/NaCl solution, at least two new effects were observed. First, the confinement effect was revealed. The more severe depolarization and faster reorientation dynamics compared to the LMPC/NaCl solution suggest a reduction of the water orientation correlation (g_K) due to the confinement environment, which reproduces the results of recent DRS [1] and simulation study [7]. Second, the non-bulk-like NaCl effect was revealed. Increase of permittivity and retardation of collective reorientation dynamics than prediction were observed near the physiological NaCl concentration (<0.3 M). Since the outside of MLV can be assumed to be a bulk NaCl solution, these deviations are due to the nanoconfined NaCl solution inside the MLV. Since these abnormal dielectric behaviors can be artifact errors resulting from subtracting the ionic conductivity term from the total dielectric loss (Chapter 5.1), we cross-checked the NaCl effect on permittivity which has no such artifact error (equation 3.5). As the non-bulk-like behavior was also observed in permittivity in DMPC/NaCl solution (Figure 5.10), the anomalous dielectric behavior in nanoconfined NaCl solution is considered as no analysis error.

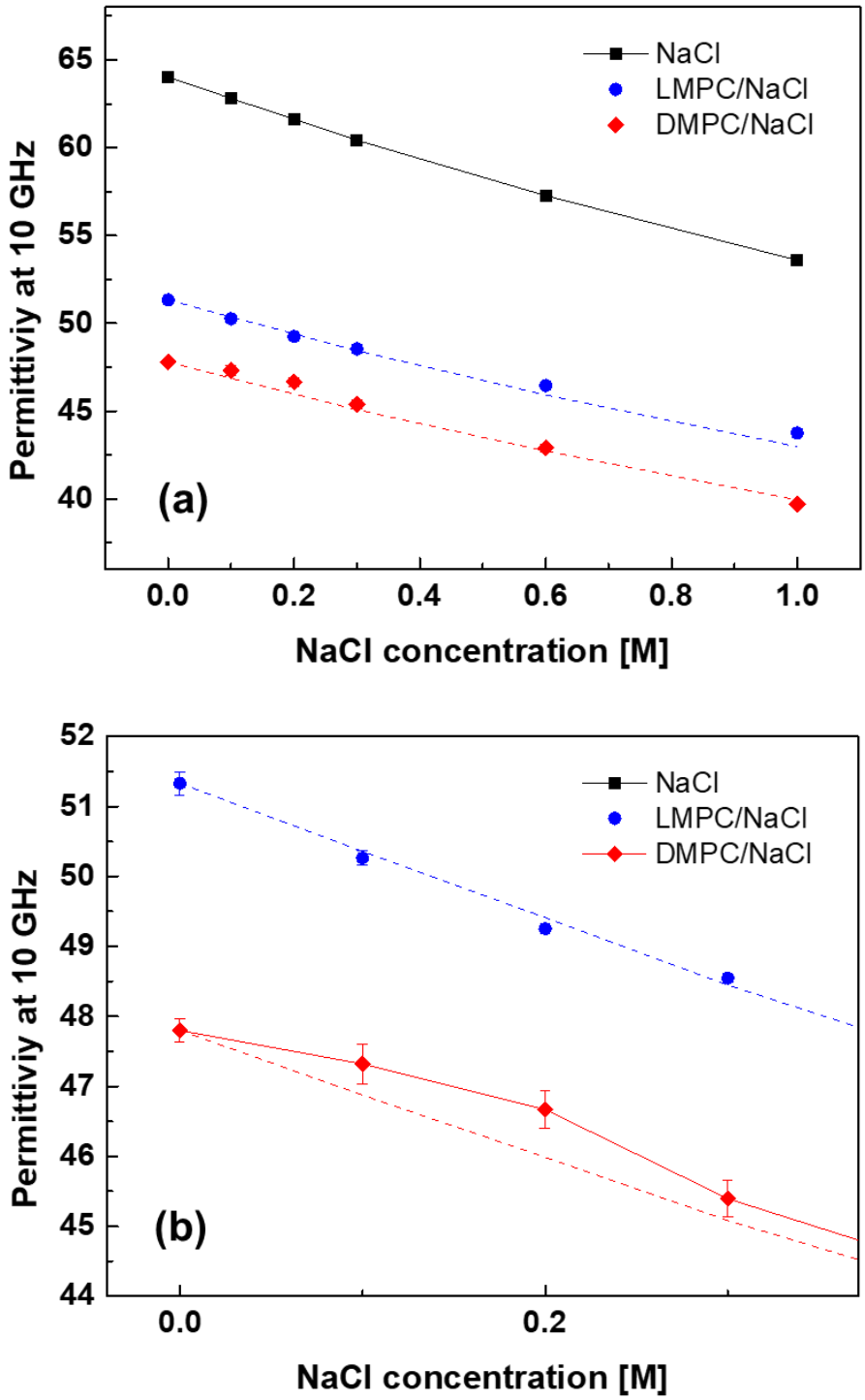

Figure 5.10 (a) Change of permittivity of all samples at 10 *GHz* with NaCl concentration, (b) Focus on NaCl low concentration.

Although anomalous dielectric behaviors of bulk mode are observed in raw data,

the “bulk mode” merely represent the averaged water dynamics inside and outside MLVs. Therefore, more accurate analysis focusing on nanoconfined NaCl solution is needed. In the next Chapter, we obtain the dielectric constant of confined NaCl solution by using an effective medium theory (Bruggeman mixture model).

5.3 Effective Medium Approximation

To obtain the dielectric constant inside DMPC MLVs, we used Bruggeman mixture model (Chapter 2.4.2),

$$f_{MLV}\frac{\varepsilon^*_{MLV}-\varepsilon^*_{tot}}{\varepsilon^*_{MLV}+\varepsilon^*_{tot}}+(1-f_{MLV})\frac{\varepsilon^*_{NaCl}-\varepsilon^*_{tot}}{\varepsilon^*_{NaCl}+\varepsilon^*_{tot}}=0 \tag{5.3}$$

where ε^*_{tot}, ε^*_{NaCl}, ε^*_{MLV} and f_{MLV} are dielectric constant of the DMPC/NaCl solution, outside DMPC MLVs, inside DMPC MLVs and volume fraction of DMPC MLVs, respectively. To obtain ε^*_{MLV}, f_{MLV} should be determined in advance (since ε^*_{tot} and ε^*_{NaCl} can be measured by independent experiments).

The f_{MLV} was calculated through the assumption that the MLV is sum of periodic unit cells (Figure 5.11). Unit cell is combination of one lipid and corresponding water molecules. In this case, f_{MLV} is expressed as,

$$f_{MLV}=c_l\times V_{unit}=c_l\times(v_l+n_w\times v_w) \tag{5.4}$$

where c_l, v_l, n_w and v_w are the lipid concentration, volume of a lipid, the number of water molecules per lipid inside MLV and volume of a water molecule, respectively.

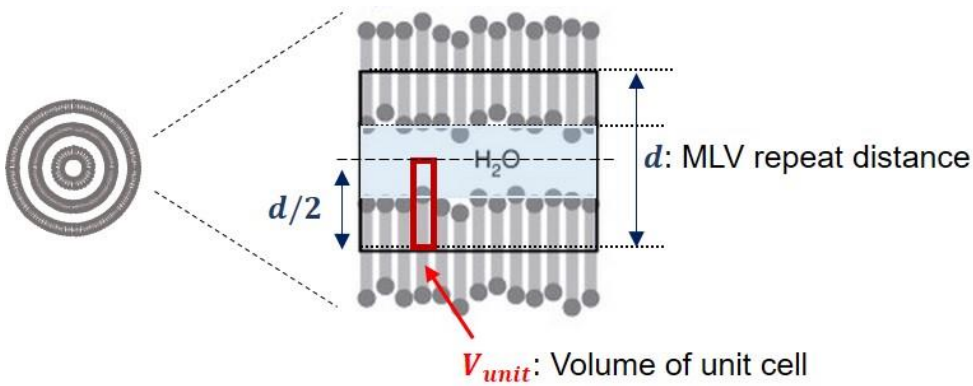

Figure 5.11. Structure inside MLV: MLV is composed by periodic unit cells

To determine f_{MLV} in 5.4, the only unknown parameter is n_w (all other

parameters are obtained by density measurements). Previous literature studies have revealed that n_w ranges from 25 to 40 for DMPC/water system [8-10]. In this thesis we used two methods for determining f_{MLV} in DMPC/NaCl solution.

(1) Centrifugation: Unlike transparent solvents, DMPC MLV is visually opaque, so f_{MLV} can be estimated through centrifugation. At the NaCl low concentration ($c \leq 0.3\ M$), opaque MLVs sink because density of MLVs is larger than solvent (NaCl aqueous solution). In this case, f_{MLV} was indirectly estimated by extracting the floating solvent (NaCl solution) with a micro pipette and measuring the volume (Figure 5.12a). However, at the NaCl high concentration ($\mathrm{c} = 0.6, 1$ M), since the density of MLVs is larger than solvent, it was impossible to extract the solvent, and f_{MLV} could not be estimated (Figure 5.12b). Figure 5.13 represent the comparison between results of centrifugation and our calculation (when $25 \leq n_w \leq 39$). When we suppose MLV is spherical shapes and all MLVs are mono sized, f_{MLV} is about 74 % of the volume fraction obtained by centrifugation.

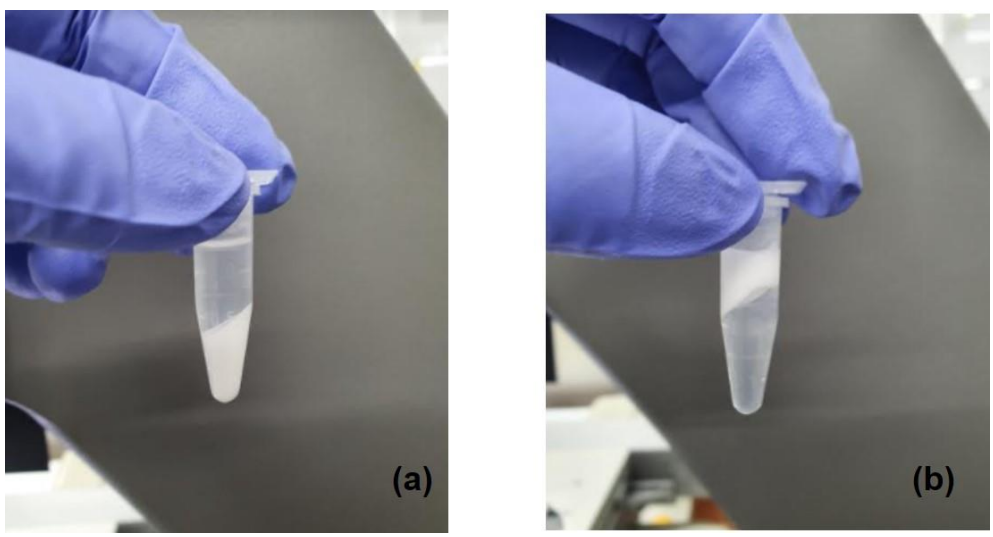

Figure 5.12. After centrifugation of DMPC/NaCl solution: (a) In 0.3 M NaCl solution, (b) In 0.6 M NaCl solution

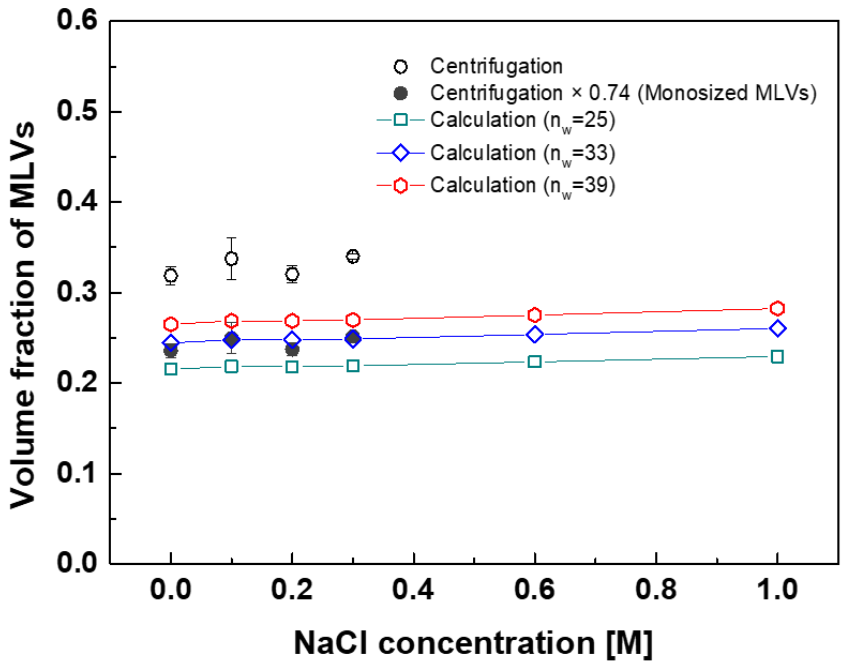

Figure 5.13. f_{MLV} **obtained by two different methods**

In the real situation, as MLVs have size distribution, f_{MLV} will have a value between 74% and 100% of the centrifugation result. Therefore, f_{MLV} from the calculation under two conditions ($n_w = 33, 39$) was considered proper.

(2) Fitting analysis of Debye relaxation models: We investigated what condition of n_w gives ε^*_{MLV} that best satisfies the Debye relaxation model at microwave frequencies. Figure 5.14 represents ε^*_{MLV} obtained using Bruggeman mixture approximation with tree conditions of n_w. Solid line represent fitting by four Debye relaxation model (Equation 5.2). In the condition of $n_w = 39$, ε^*_{MLV} shows the most consistent result with the fitting line.

Further analysis of dielectric relaxation behavior on ε^*_{MLV} is discussed in the next Chapter.

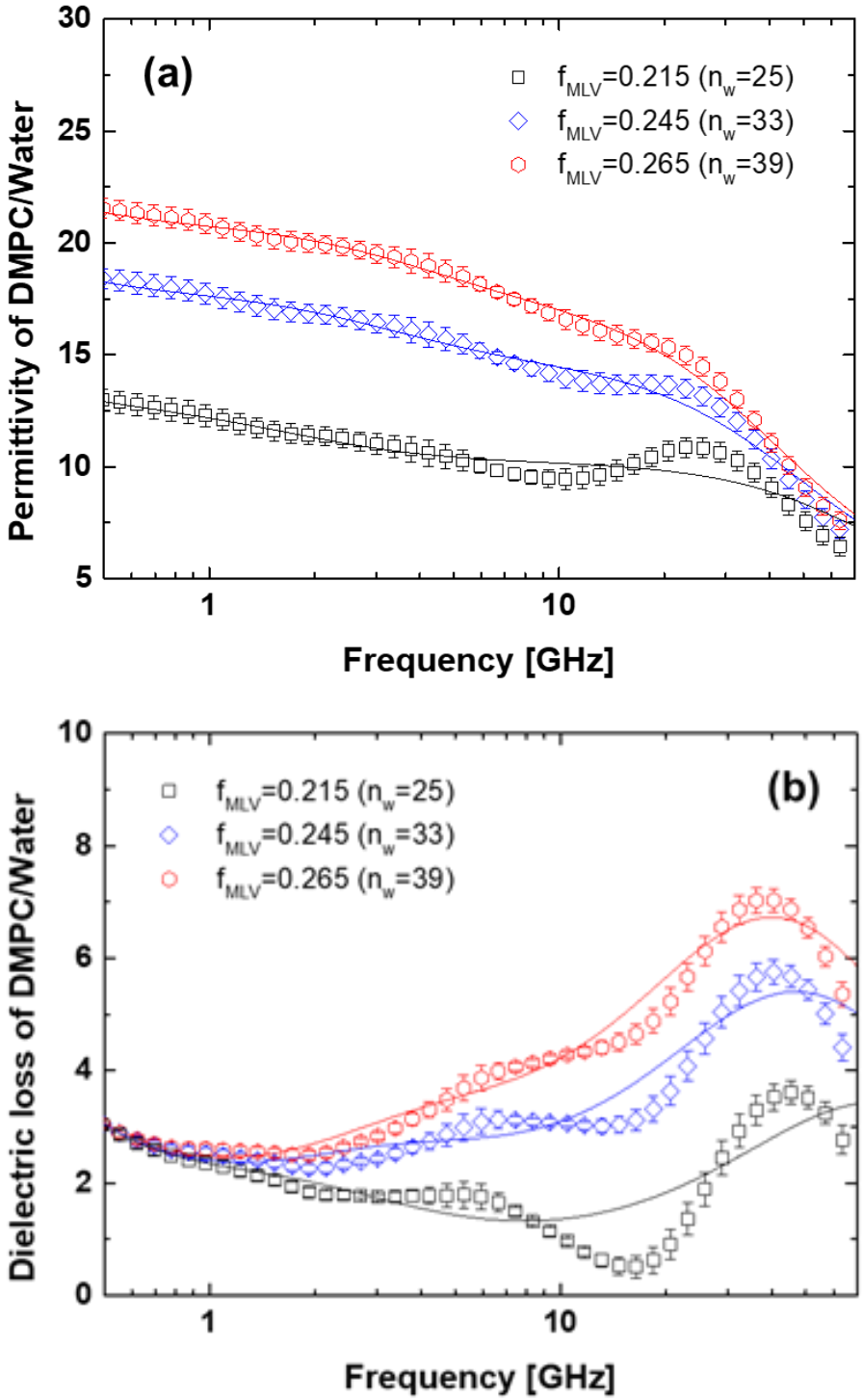

Figure 5.14. ε^*_{MLV} obtained from Bruggeman mixture model with three difference conditions. (a) Permittivity, (b) Dielectric loss. Solid line: Fitting by four Debye relaxation model.

5.4 Anomalous Increase of Dielectric Constant of Nanoconfined NaCl Solution (In DMPV MLV)

Permittivity and dielectric loss of MLV in DMPC/NaCl solution obtained from the Bruggeman mixture approximation (described in Chapter 5.3) is depicted in Figure 5.15. To analyze dielectric behaviors of nanoconfined NaCl solution, we simultaneously fitted permittivity (ε'_{MLV}) and dielectric loss (ε''_{MLV}) by four Debye relaxation model. The relaxation time of DMPC lipid (τ_s) was held fixed at the literature value, 4000 ps [3].

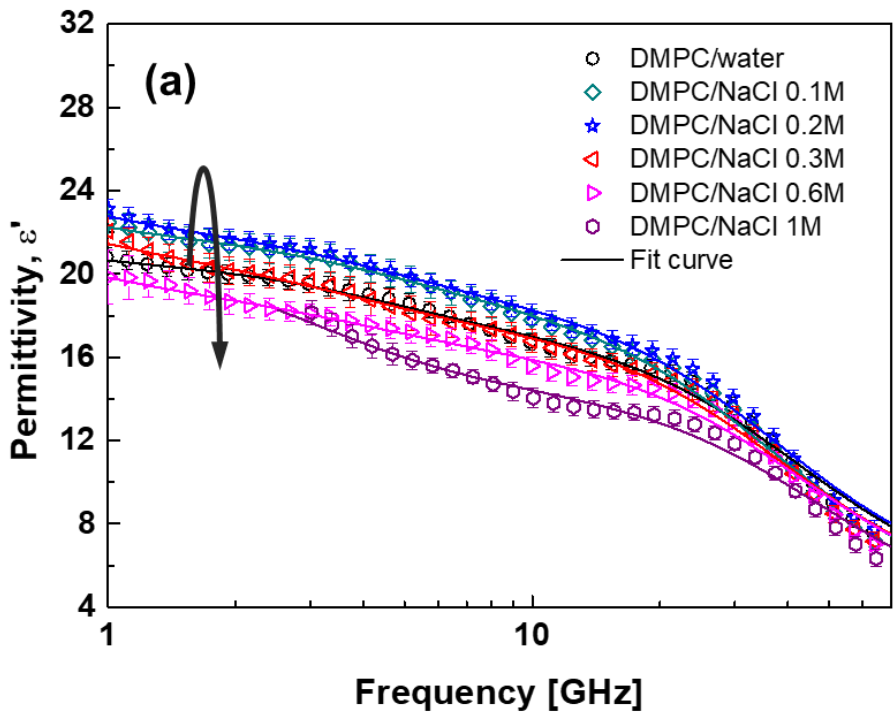

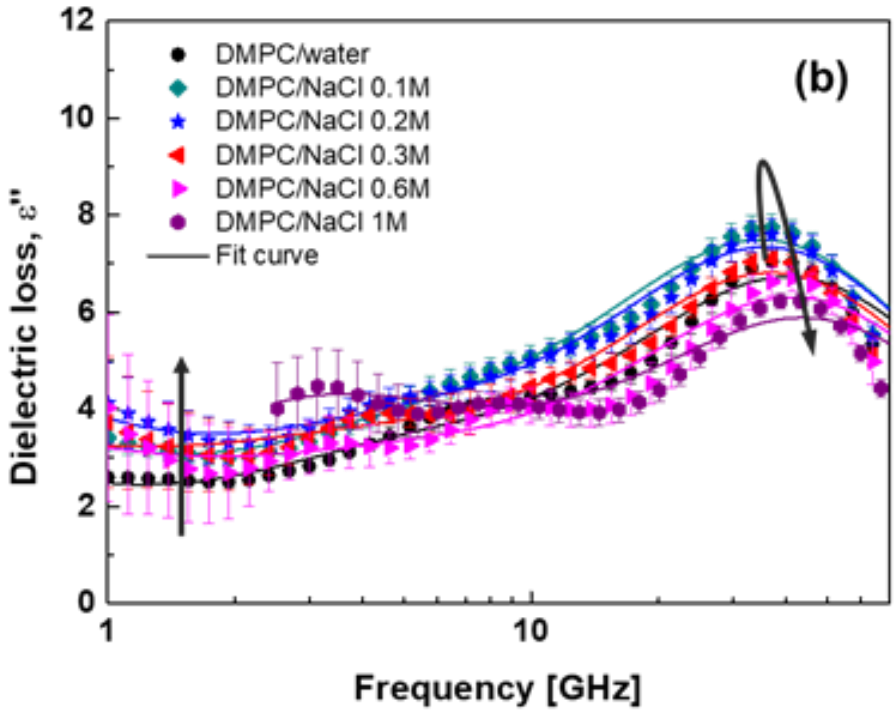

Figure 5.15. (a) Permittivity and (b) Dielectric loss spectrum of DMPC MLV for different NaCl concentrations obtained by Bruggeman mixture model (Solid line: Four Debye fitting result).

Figure 5.16 represents a static permittivity for NaCl solution confined in DMPC MLV. Since Bruggeman analysis gives the dielectric behavior of the entire MLV, the permittivity obtained is less than that of the confined NaCl solution by the volume of the lipid molecules, so this effect was corrected (red open diamond). Interestingly, an increase in static permittivity of nanoconfined NaCl solution was observed, especially near the physiological NaCl concentrations (<0.3 M). Such effect was also confirmed in the permittivity spectrum of MLV (Figure 5.15a). Although abnormal enhancement of permittivity has been consistently predicted in molecular dynamics simulation studies [11-13], to the author's knowledge, experimental evidence is still lacking. Therefore, our study suggests a first experimental evidence of anomalous dielectric constant in the nanoconfined NaCl solution [14].

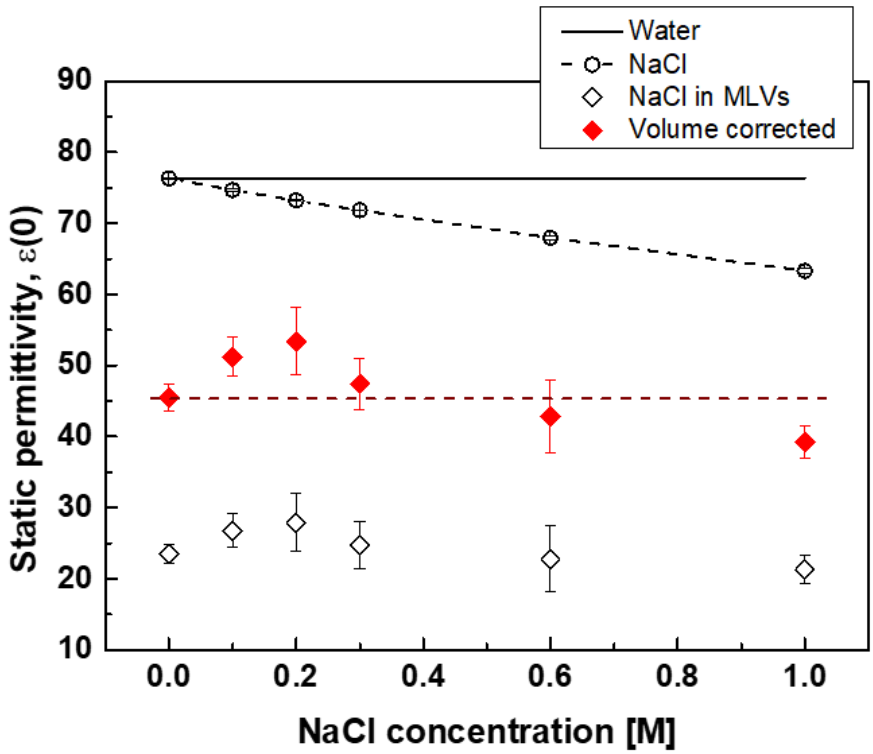

Figure 5.16. Static permittivity for NaCl solution confined in DMPC MLV (Black open diamond) and volume corrected value (red filled diamond). The dark red dashed line denotes a value of nanoconfined water (~ 45.5). Values for water and bulk NaCl solution were also represented (Black solid line and black open circle, respectively).

5.5 Interpretation

Since MLV is an isotropic spherical platform [15], the measured static permittivity (Figure 5.16) is the result of averaging the dielectric constant components parallel ($\varepsilon_{\parallel}$) and perpendicular ($\varepsilon_{\perp}$) to the MLV membrane surface (Figure 5.17). When the anisotropic dielectric components of nanoconfined NaCl solution between two graphene layers of the previous simulation study [13] are roughly averaged as $(\varepsilon_{\perp} + \varepsilon_{\parallel})/2$, the result shows almost similar trend to our data, increased permittivity below 0.5 M NaCl concentration (Figure 5.18). Therefore, the origin of enhanced permittivity in Figure 5.16 is suggested as an increase in the dielectric component perpendicular to the membrane surface as the previous simulation proposed [13].

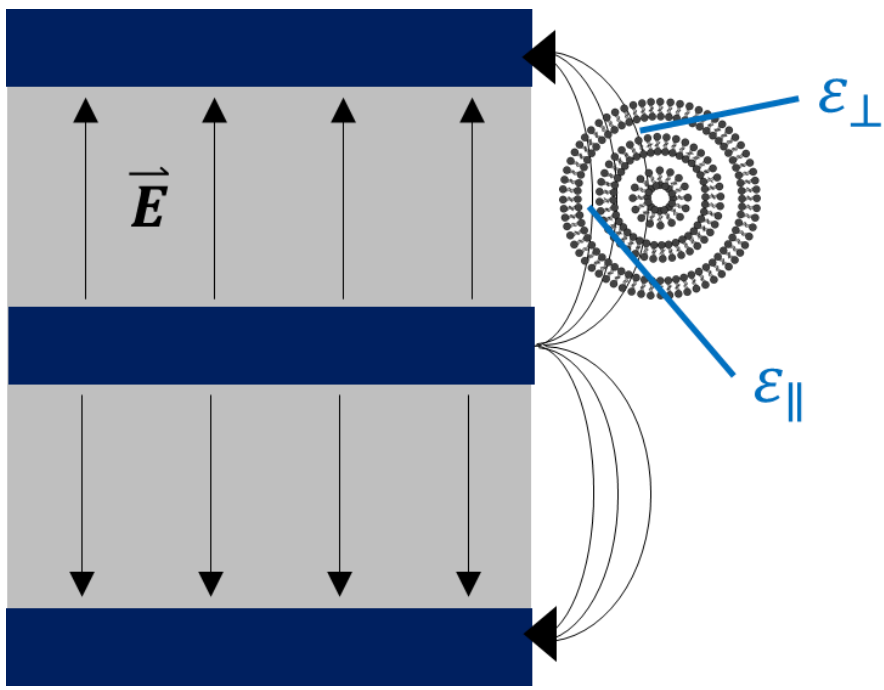

Figure 5.17. Open-ended coaxial probe method measures "average" of all dielectric components in DMPC MLVs.

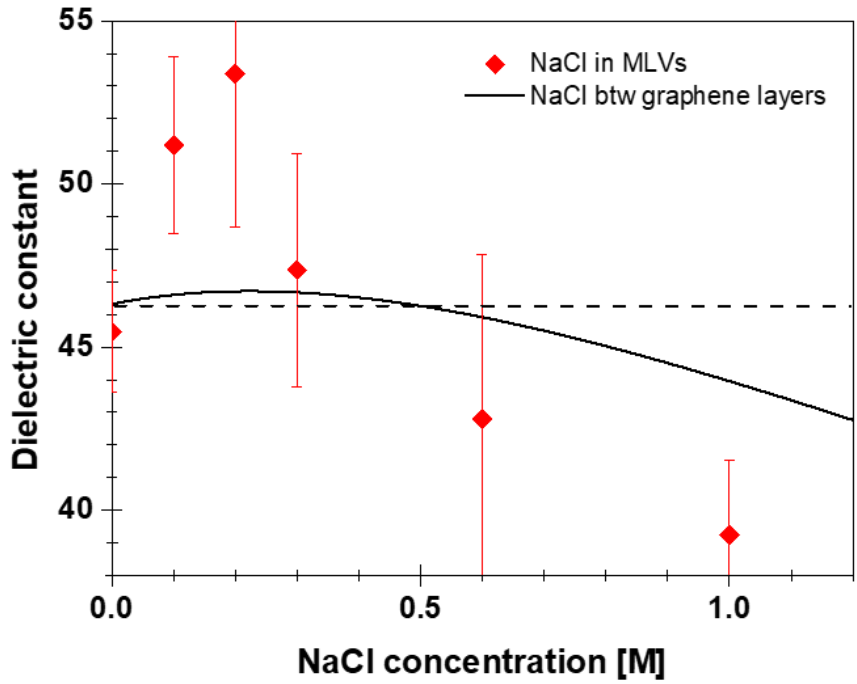

Figure 5.18. Static permittivity of our data (NaCl in MLVs, red diamond) is compared to $((\varepsilon_{\perp} + \varepsilon_{\parallel})/2)$ of nanoconfined NaCl solution btw two graphene layers [13].

Bibliography

1. Eom, K. Collective dynamics of nanoconfined water studied by broadband dielectric relaxation spectroscopy. Chapter 4 Ph.D. thesis, Seoul National University, **2019**.
2. George, D. K.; Charkhesht, A.; Hull, O. A.; Mishra, A.; Capelluto, D. G. S.; Mitchell-Koch, K. R.; Vinh, N. Q., *J. Phys. Chem. B* **2016,** *120* (41), 10757-10767.
3. Klosgen, B., *Biophys. J.* **1996,** *71*, 3251-3260.
4. Pabst, G.; Hodzic, A.; Strancar, J.; Danner, S.; Rappolt, M.; Laggner, P., *Biophys. J.* **2007,** *93* (8), 2688-96.
5. Valley, C. C.; Perlmutter, J. D.; Braun, A. R.; Sachs, J. N., *J. Membr. Biol.* **2011,** *244* (1), 35-42.
6. Rinne, K. F.; Gekle, S.; Netz, R. R., *J. Phys. Chem. A* **2014,** *118* (50), 11667-77.
7. Honegger, P.; Schmollngruber, M.; Steinhauser, O., *Phys. Chem. Chem. Phys.* **2018,** *20* (16), 11454-11469.
8. Nagle, J. F.; Tristram-Nagle, S., *Biochim. Biophys. Acta* **2000,** *1469* (3), 159-195.
9. Costigan, S. C.; Booth, P. J.; Templer, R. H., *Biochim. Biophys. Acta* **2000,** *1468* (1-2), 41-54.
10. Hishida, M.; Tanaka, K., *Phys. Rev. Lett.* **2011,** *106* (15), 158102.
11. Zhu, H.; Ghoufi, A.; Szymczyk, A.; Balannec, B.; Morineau, D., *Phys. Rev. Lett.* **2012,** *109* (10).
12. Renou, R.; Szymczyk, A.; Ghoufi, A., *Nanoscale* **2015,** *7* (15), 6661-6666.
13. Jalali, H.; Lotfi, E.; Boya, R.; Neek-Amal, M., *J. Phys. Chem. B* **2021,** *125* (6), 1604-1610.
14. Jang, J.; Kim, S.; Eom, K., *Chem. Phys. Lett.* **2021,** *780*, 138912.
15. Sauvage, F.; Legrand, F.-X.; Roux, M.; Rajkovic, I.; Weiss, T. M.; Varga, Z.; Augis, L.; Nugue, G.; Debouzy, J.-C.; Vergnaud-Gauduchon, J.; Barratt, G., *J. Colloid Interface Sci.* **2019,** *537*, 704-715.

Chapter 6.
Molecular Mechanism of NaCl Effect on Dielectric Constant of Nanoconfined Water in MLVs

6.1 For Membrane-Surface Bound Water

To study the molecular mechanism of dielectric enhancement in nanoconfined NaCl solution, dielectric strength and collective reorientation time of both membrane surface-bound water and water beyond the hydration layer have been analyzed (Chapter 6.1 and 6.2, respectively). It has been known that there are two kinds of bound water in phosphatidylcholine (PC) lipid, tightly bound water which is H-bonded to phosphate or carbonyl head group, and weakly bound water which is electrically attracted to choline head group [1-2]. The relaxation time of tightly bound water in DMPC/water is about 508 ± 133 ps (Figure 6.1b) which is in good agreement with the result of MHz DRS [3]. NaCl accelerates the reorientation dynamics and enhances permittivity of tightly bound water, (Figure 6.1a and 6.1b, respectively) suggesting the fact that Na^+ binds to the phosphate or carbonyl group, which consistent with results in calorimetry [4] and simulations [5-6], and affects surrounding hydration water. NaCl-induced acceleration of reorientation motion of bound water, which is in line with enhanced translational diffusion measured by Overhauser dynamic nuclear polarization (ODNP) [7], suggests that Na^+ perturbs H-bond between tightly bound water and lipid head group (Figure 6.3). In other words, the Na^+ perturbation effect enhances the rotational degree of freedom of water surrounding the phosphate or carbonyl group and consequently increases the permittivity. This scenario is consistent with the suggestion from previous simulations [8-10]. On the other hand, NaCl has negligible effects on the dynamics of weakly bound water (Figure 6.1b), suggesting that Cl^- does not directly bind to the choline group, consistent with simulations' prediction [5-6]. The decrease in the weakly bound mode strength (Figure 6.1a) implies that the number of weakly bound water molecules is reduced by being included in the surrounding Na^+ hydration shell. NaCl effect on bound waters in LMPC/NaCl solution is in good agreement with that

in DMPC/NaCl solution (Figure 6.2), which is reliable since two lipids have an identical head group structure.

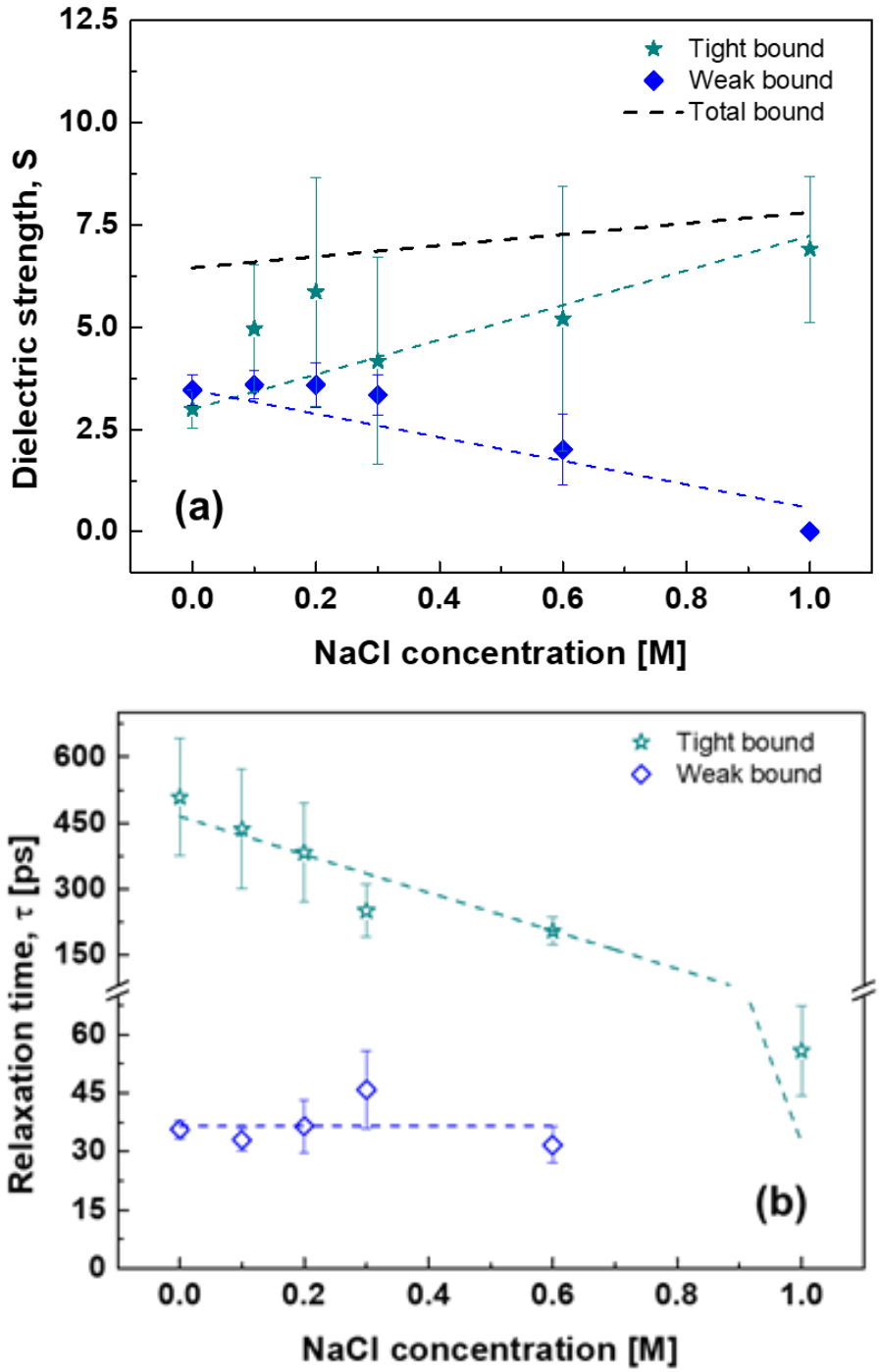

Figure 6.1. (a) Dielectric strengths and (b) relaxation times of both tightly and weakly bound water for NaCl solution inside DMPC MLV, respectively.

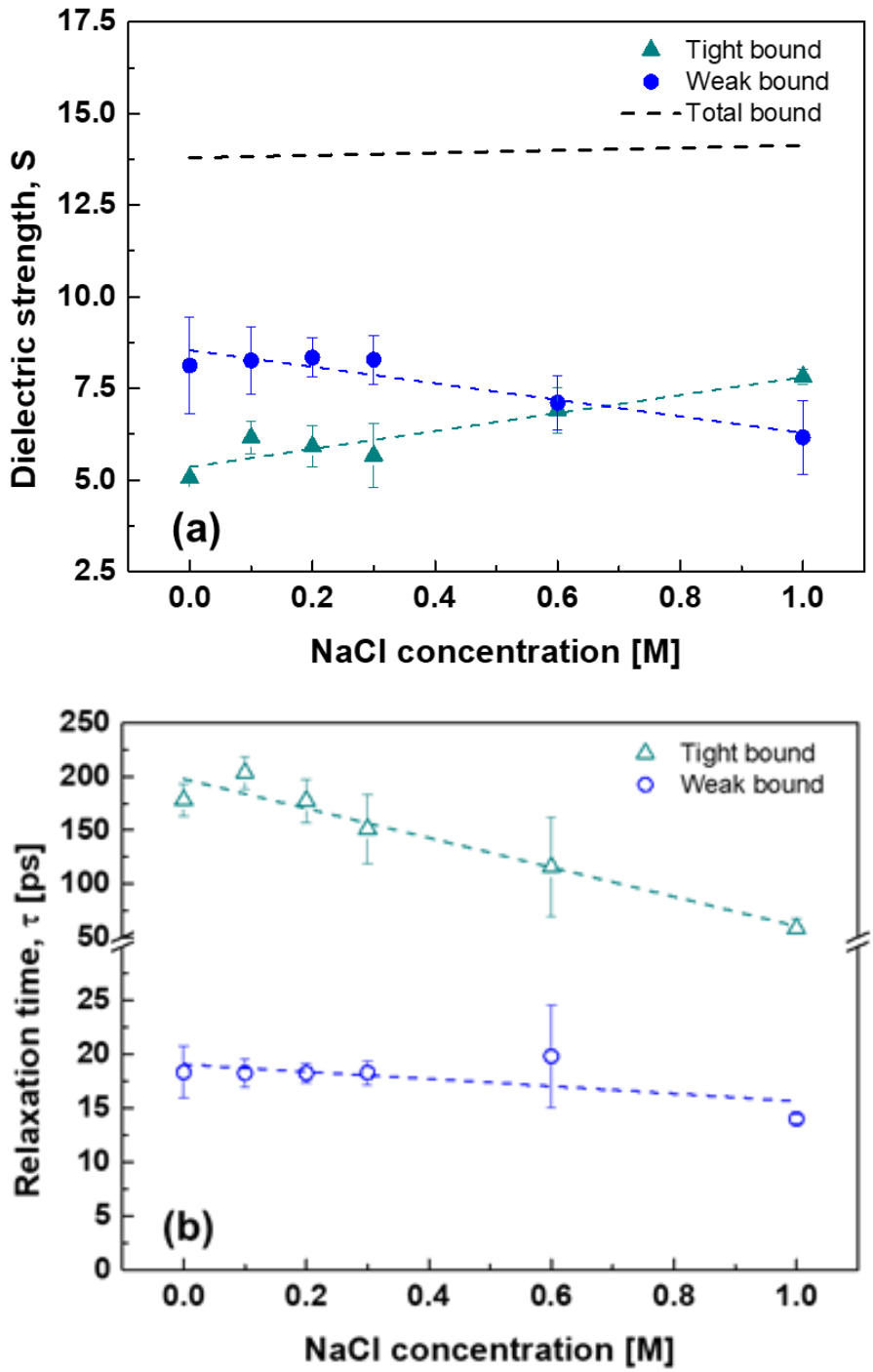

Figure 6.2. (a) Dielectric strengths and (b) relaxation times of both tightly and weakly bound water for LMPC/NaCl solution, respectively.

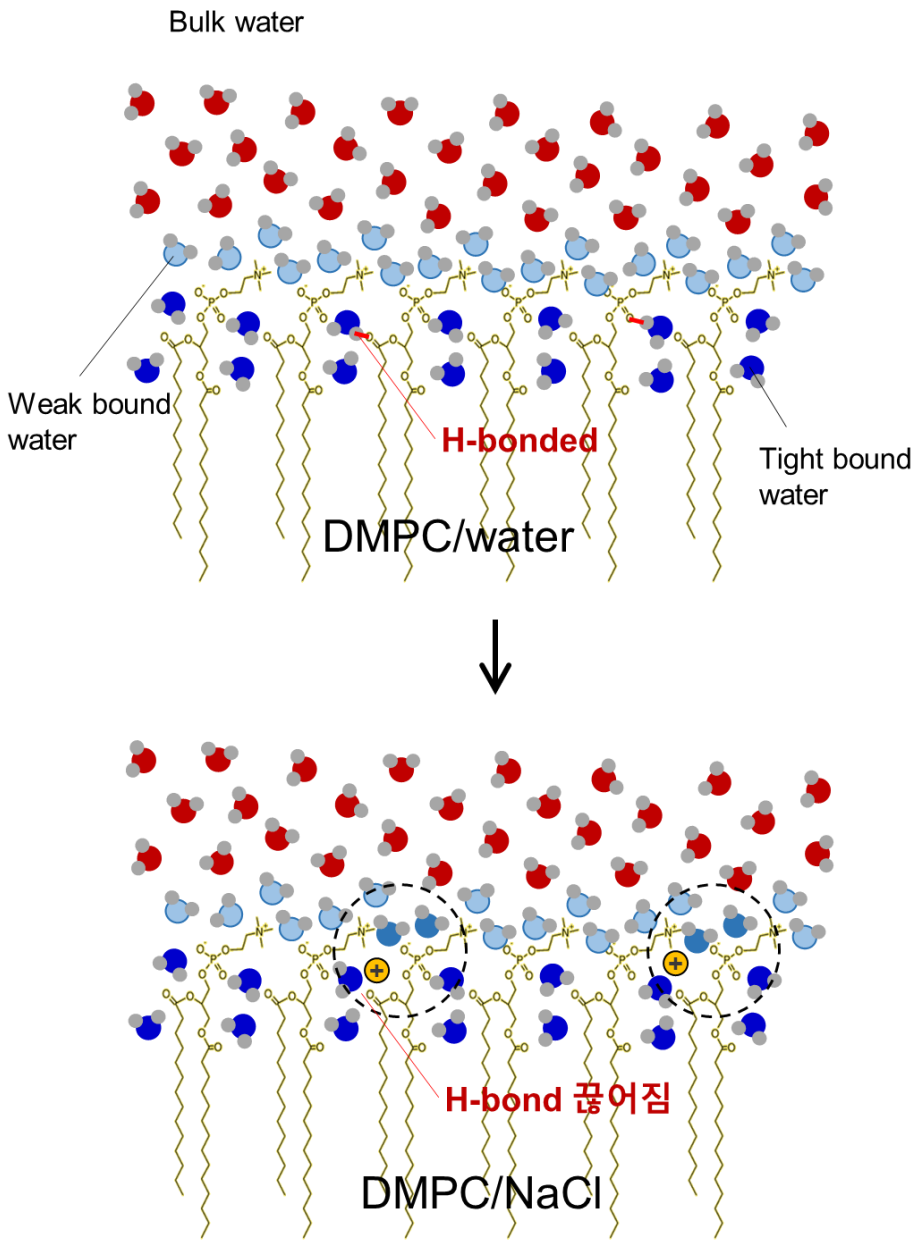

Figure 6.3. Schematics of NaCl effect on tightly bound water of DMPC membrane.

6.2 For Water beyond Membrane Hydration Layer

NaCl effect on water beyond the membrane hydration layer is depicted in Figure 6.4. NaCl enhances dielectric strength near the ion physiological concentration ($0 < c < 0.3$ M) and the origin can be guessed as an increase of dielectric element perpendicular to the membrane surface (Chapter 5.5). However, contrary to surface-bound water, the retardation of collective reorientation motion was observed (Figure 6.4a). Therefore, for water beyond the hydration layer, the mechanism of increased permittivity is not the enhanced rotational degree of freedom. Strong dipole-dipole interaction between water molecules induces orientationally correlated-structure, which effectively enhances permittivity of the system. So, origin of anomalous increase of permittivity was tried to be interpreted in terms of change of orientation correlation of water beyond hydration layer.

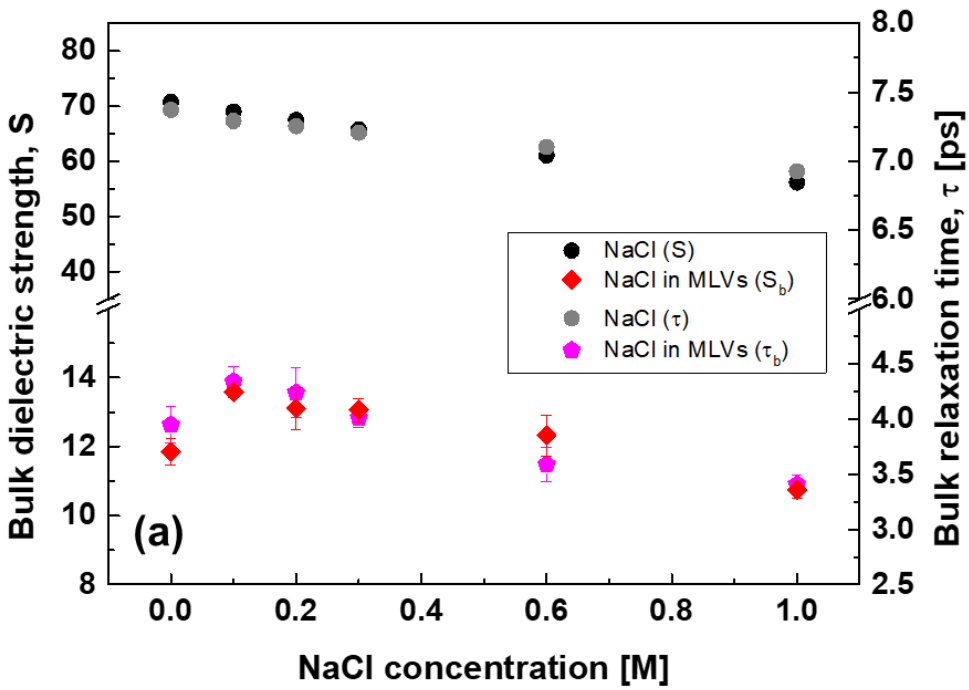

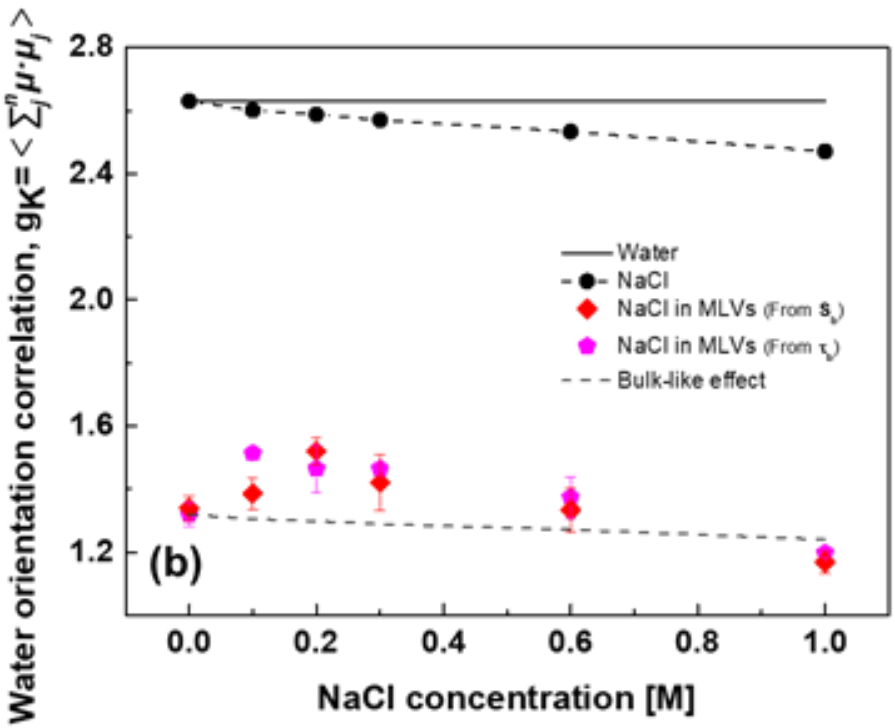

Figure 6.4. (a) Dielectric strengths, relaxation times, and (b) Kirkwood factor of water beyond the membrane-surface bound water for NaCl solution confined in DMPC MLV. Data for NaCl in the bulk system is also represented.

From the Kirkwood-Froelich theory, the dielectric strength, S, is proportional to the Kirkwood factor, g_K $(= \langle \sum_j^n \hat{\mu} \cdot \hat{\mu}_j \rangle)$ [11-12],

$$S = \varepsilon_s - \varepsilon_\infty = \frac{g_K N \mu^2}{9 k_B T \varepsilon_0} \frac{\varepsilon_s (\varepsilon_\infty + 2)^2}{(2\varepsilon_s + \varepsilon_\infty)} \qquad \text{(eq. 5)}$$

where N, μ, k_B, T, ε_0, ε_s, and ε_∞ are the number of bulk water molecules, the dipole moment of water in the gaseous state, Boltzmann's constant, temperature, vacuum permittivity, static permittivity, and high-frequencypermittivity, respectively. N inside MLVs was calculated from the relation, $N = N_{tot} - c_{lip} N_{hyd}$, where N_{tot}, c_{lip}, and N_{hyd} are the total number of water in MLVs, the concentration of DMPC, and hydration number, respectively. For the N_{hyd}, results from our previous study [13] and quasi-elastic neutron scattering (QENS) [14] ($N_{hyd} = 12$) were used.

In addition, correlated-structure delays the dielectric relaxation of water dipoles. From the Kivelson-Madden equation, collective relaxation time, τ_{DRS}, is proportional to the g_K [11, 15],

$$\tau_{DRS} \approx g_K \tau_{single} \qquad \text{(eq. 6)}$$

where τ_{single} is single molecular reorientation time. We supposed that $\tau_{single}(c) \approx \tau_{single}(0)$ where c is salt concentration because previous simulation has suggested NaCl negligibly affects τ_{single} of surrounding water dipoles [16]. g_K beyond the surface-hydration water in MLVs are depicted in Figure 6.4b. Calculation from two different parameters shows almost identical results. NaCl reduces the correlation of the surrounding water in the bulk system, but rather increases it in the confinement environment near ion physiological concentration, from g_k=1.3 to 1.5 (15% enhanced). This fact suggests that the mechanism by which NaCl increases the permittivity differs in two water regions (in and beyond the surface-bound waters), and the origin on the latter is change of intermolecular orientation correlation, not a rotational degree of freedom of individual molecules. Recently, it has been known that nanoconfinement reduces water correlation (g_K) [13, 15]. The strongly oriented surface-bound water may break the surrounding water-water network and correlation. In the nanoconfined NaCl solution, Cl^- ions accumulated around membrane surface may act as a defect, blocking strong interaction between surface-bound water and surrounding water, thereby restoring the water-water correlation beyond the interface (Figure 6.5).

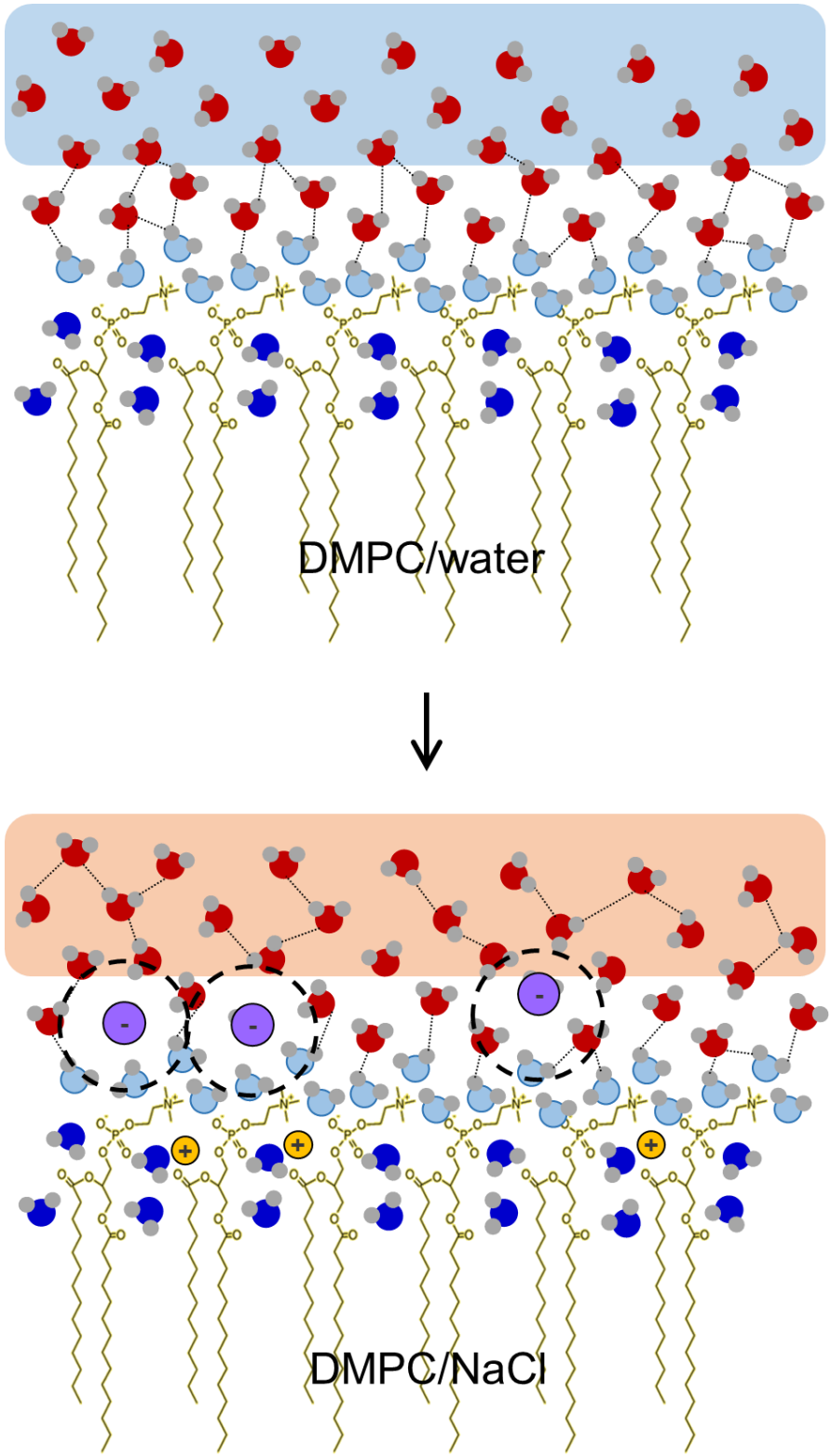

Figure 6.5. Schematics of NaCl effect on intermolecular orientation correlation beyond membrane hydration layer.

Bibliography

1. George, D. K.; Charkhesht, A.; Hull, O. A.; Mishra, A.; Capelluto, D. G. S.; Mitchell-Koch, K. R.; Vinh, N. Q., *J. Phys. Chem. B* **2016,** *120* (41), 10757-10767.
2. Volkov, V. V.; Nuti, F.; Takaoka, Y.; Chelli, R.; Papini, A. M.; Righini, R., *J. Am. Chem. Soc.* **2006,** *128* (29), 9466-9471.
3. Klosgen, B., *Biophys. J.* **1996,** *71*, 3251-3260.
4. Knecht, V.; Klasczyk, B., *Biophys. J.* **2013,** *104* (4), 818-24.
5. Pandit, S. A., *Biophys. J* **2003,** *84*, 3743–3750.
6. Ishiyama, T.; Shirai, S.; Okumura, T.; Morita, A., *J. Chem. Phys.* **2018,** *148* (22), 222801.
7. Song, J.; Franck, J.; Pincus, P.; Kim, M. W.; Han, S., *J. Am. Chem. Soc.* **2014,** *136* (6), 2642-2649.
8. Zhu, H.; Ghoufi, A.; Szymczyk, A.; Balannec, B.; Morineau, D., *Phys. Rev. Lett.* **2012,** *109* (10).
9. Renou, R.; Szymczyk, A.; Ghoufi, A., *Nanoscale* **2015,** *7* (15), 6661-6666.
10. Jalali, H.; Lotfi, E.; Boya, R.; Neek-Amal, M., *J. Phys. Chem. B* **2021,** *125* (6), 1604-1610.
11. Kaatze, U., *J. Chem. Phys.* **2017,** *147* (2), 024502.
12. Bottcher, C. J., *Theory of Electric Polarization, Vol.1 Dielectrics in Static Fields*. 2nd ed.; Ch. 6 Elsevier, Amsterdam: **1973**.
13. Eom, K. Collective dynamics of nanoconfined water studied by broadband dielectric relaxation spectroscopy. Chapter 4 Ph.D. thesis, Seoul National University, **2019**.
14. Yamada, T.; Takahashi, N.; Tominaga, T.; Takata, S.-I.; Seto, H., *J. Phys. Chem. B* **2017,** *121* (35), 8322-8329.
15. Honegger, P.; Schmollngruber, M.; Steinhauser, O., *Phys. Chem. Chem. Phys.* **2018,** *20* (16), 11454-11469.
16. Rinne, K. F.; Gekle, S.; Netz, R. R., *J. Phys. Chem. A* **2014,** *118* (50), 11667-77.

Chapter 7.
Conclusion

In this study, the NaCl effect and its molecular mechanism on the dielectric constant of nanoconfined water in phospholipid MLV are investigated. Anomalous NaCl effect, i.e., an increase of static permittivity was observed, which has been consistently suggested by simulations, but to the author's knowledge, is the first experimental evidence. NaCl accelerates reorientation motion and enhances the permittivity of membrane surface-bound water. This observation suggests NaCl enhances the rotational degree of freedom of bound water, which is consistent with the previous simulations. However, NaCl retards the collective reorientation dynamics of water beyond the membrane hydration layer, which was interpreted as enhanced water orientation correlation. In conclusion, the mechanism by which NaCl increases the permittivity differs in membrane surface-bound water and beyond bound water, and the origin on the latter is a change in intermolecular correlation, not rotational freedom of individual molecules.

국문 초록

본 연구에서 우리는 GHz 유전체 이완 분광법 (DRS)을 사용하여 NaCl이 인지질 다층 구조 (MLV) 내부의 나노공간에 갇힌 물의 유전 상수를 향상 시킨다는 첫 번째 실험 증거를 제시하였다. 이러한 현상은 벌크 환경 (벌크 NaCl 용액 및 인지질 미셀 / NaCl 용액)에서는 관찰되지 않았으며, 단지 이온 농도가 증가함에 따라 유전 상수의 단조 감소가 나타났다. NaCl은 MLV에 갇힌 물의 유전 상수의 비선형 변화, 즉 생리적 이온 농도 근처에서 이례적인 증가 ($0 < c < 0.3$ M) 및 고농도에서의 감소 ($0.3 < c < 1$ M)를 유도하였다. 이전 시뮬레이션 연구들의 결과와 비교할 때, 이 비선형 유전 거동은 NaCl에 의해 유도 된 세포막 표면에 수직한 유전 성분 ($\varepsilon_{\perp}$)의 증가와 평행한 유전 성분 ($\varepsilon_{\parallel}$)의 감소 사이의 경쟁의 결과로 해석된다. .

또한 이례적인 NaCl 효과의 분자 메커니즘도 조사되었다. NaCl은 MLV 내에서 두 물의 영역, 즉 세포막 표면에 결합한 물과 그 너머의 물의 유전 상수를 다른 방식으로 향상시킨다. 표면 결합 물의 가속된 집합적 재배향 운동이 관찰되었으며, 이는 회전 자유도의 증가를 의미한다. 그러나 세포막 수화 층을 넘어서는 물의 경우 더 느린 집단 운동과 유전 상수의 증가가 동시에 관찰되었고, 이는 NaCl이 개별 물 분자의 회전 자유도 보다 분자간 배향 상관 관계 (또는 Kirkwood 상관 계수, gK)를 향상시킨다는 것을 시사한다.

핵심어: 나노공간에 갇힌 물, NaCl, 유전 상수, 인지질, Kirkwood 상관계수, 분자간 방향 상관관계, 유전체 이완 분광법

학번: 2016-30098